



Inverse modelling for real-time estimation of radiological consequences in the early stage of an accidental radioactivity release



Petr Pecha*, Václav Šmídl

Institute of Information Theory and Automation of the Czech Academy of Sciences, v.v.i., Pod Vodarenskou vezi 4, 182 08, Prague 8, Czech Republic

ARTICLE INFO

Article history:

Received 8 October 2015
Received in revised form
14 May 2016
Accepted 19 June 2016

Keywords:

Radioactivity release
Assimilation of measurements
Ill-posed inversion problem
Measurement noise
Urgent emergency

ABSTRACT

A stepwise sequential assimilation algorithm is proposed based on an optimisation approach for recursive parameter estimation and tracking of radioactive plume propagation in the early stage of a radiation accident. Predictions of the radiological situation in each time step of the plume propagation are driven by an existing short-term meteorological forecast and the assimilation procedure manipulates the model parameters to match the observations incoming concurrently from the terrain. Mathematically, the task is a typical ill-posed inverse problem of estimating the parameters of the release. The proposed method is designated as a stepwise re-estimation of the source term release dynamics and an improvement of several input model parameters. It results in a more precise determination of the adversely affected areas in the terrain. The nonlinear least-squares regression methodology is applied for estimation of the unknowns. The fast and adequately accurate segmented Gaussian plume model (SGPM) is used in the first stage of direct (forward) modelling. The subsequent inverse procedure infers (re-estimates) the values of important model parameters from the actual observations. Accuracy and sensitivity of the proposed method for real-time forecasting of the accident propagation is studied. First, a twin experiment generating noiseless simulated “artificial” observations is studied to verify the minimisation algorithm. Second, the impact of the measurement noise on the re-estimated source release rate is examined. In addition, the presented method can be used as a proposal for more advanced statistical techniques using, e.g., importance sampling.

© 2016 Elsevier Ltd. All rights reserved.

1. Introduction

Measured and calculated doses/dose rates of external irradiation induced by radioactive cloud propagation are basic inputs to the objective analysis of the data assimilation (DA) techniques. The aim of DA is modification of the internal parameters of a dispersion model in order to obtain a good fit of the model predictions with observations incoming from the terrain. The task is solved as an inversion problem when the values of certain model parameters must be refined inversely from the observed data. The inversion of the original forward problem is a valuable tool for improvement of the important model parameters, primarily for the source strength re-estimation and the parameters controlling the recursive tracking of the plume progression at small distances from the source. Source term analysis based on operational conditions can occasionally be impossible due to the potential blackout of a nuclear power station,

in which case the inverse modelling based on the radiation monitoring becomes a sole solution. The uncertainty in the source term dominates among all other uncertainties of an accidental release scenario. Estimated radiological values can differ from the true ones by a factor of 10 or more. Proper re-estimation can significantly contribute to more accurate localisation of the most impacted areas in the terrain. In principle, the assimilation procedures require the most accurate data possible, to be obtained from measuring devices (sensors) located on the terrain around the perimeter of a nuclear facility and an additional network of the measuring devices at outer distances (fixed stations, apparatus deployed temporarily on terrain in case of emergency, monitoring vehicles, aerial monitoring and other possible unmanned aerial vehicles).

We have examined the inversion problem for the category of parameter estimation where the system characteristics are inferred from the experimental data. Inverse problems are often mathematically ill-posed (improperly posed) due to an information deficit (e.g., <http://www.waterloo.ca>, Kabanikhin, 2008). It is called an inverse problem because it starts with the effects and then

* Corresponding author.

E-mail address: pecha@utia.cas.cz (P. Pecha).

calculates the causes. This is the inverse of the original forward problem, which starts with the causes and then calculates the effects. The solution of an ill-posed problem is often not unique and gives rise to instability with respect to measurement errors or small changes in the data. When sufficiently informative measurements are available, the inversion step typically provides a unique solution. However, this is not guaranteed for extreme cases of the parameter correlations. Only their ratios and not their individual values can be determined then.

An overview of the assimilation methods capable of solving the inverse modelling task is given in Chapter 3. Section 3.1 provides a motivation for simple data assimilation from the perspective of advanced statistical assimilation techniques. A dispersion model can provide predictions for multiple (Monte Carlo) runs of the pollution trajectories. The likelihood of the trial for different parameterisations of the dispersion models (e.g., source term, wind velocity vector, potential precipitation, etc.) can be summarised in the form of the posterior probability distribution. The methods for nuclear source estimation are summarised, e.g., in (Rao, 2007). Some specific applications are examined using the inverse modelling technique which is widely defined (Rao, 2007) as any technique used for identifying the source from the corresponding category of measurements (e.g. dose rates). Targeting of observations using the inverse modelling technique is presented in (Abida and Bocquet, 2009) with a design strategy to seek the optimal location of mobile monitors. A semi-automatic method based on inverse modelling, proposed in (Winiarek et al., 2011), is designed for assessment of a newly planned surveillance network covering large observational errors and analysing outlying situations where the inversion could fail. The source reconstruction of an accidental radionuclide release on a continental scale is examined in (Krysta and Bocquet, 2007) where a generalised classical variational least-squares assimilation technique is tested on a set of TWIN experiments. The authors stated that a truly successful three-dimensional inversion is still far out of reach using existing computer capability.

Several remarkable articles deal with the latest experience with the Fukushima accident. In (Saunier et al., 2013) the inverse modelling procedure is combined with an attempt at reconstruction of the isotopic composition of the discharge. Examination of the emissions of two isotopes into the atmosphere, the noble gas ^{133}Xe and the aerosol-bound ^{137}Cs , was accomplished in (Stohl et al., 2012). The first guess was subsequently improved by inverse modelling, which combined the results of an atmospheric transport model FLEXPART with measurement data from several dozen stations in Japan, North America and other regions. An application to the real nuclear disaster of the Fukushima Daiichi plant is presented in (Winiarek et al., 2012). An efficient inverse modelling method is proposed there to reconstruct the Fukushima Daiichi source from the long-range transport data. The maximisation of the likelihood of publicly released measurements of the air activity concentration of radionuclides was applied. Following these top scientific activities we have obtained experience in the field. The assimilation subsystem (ASIM (2013)) in conjunction with the probabilistic version of the segmented Gaussian dispersion model SGPM has been developed and the first applications addressing the advanced Particle Filter (PF) were tested (e.g., Pecha et al., 2009; Šmídl et al., 2014). The high computational cost of the Monte-Carlo techniques can be significantly reduced when an optimisation-based first guess is used to design the proposal function (Šmídl and Hofman, 2014). In this paper, we propose an optimisation approach for the SGPM.

In Section 3.2 of this article, we propose a nonlinear least-squares regression scheme which optimises the agreement between the measured values and model prediction. Computational

efficiency of the SGPM enables generation of results in real-time mode. The use of nonlinear regression analysis for integrating pollutant concentration measurements with an atmospheric dispersion model for source term estimation can be found in (Edwards et al., 1993). The inverse model as a nonlinear least squared estimation is presented in (Kathirgamanathan et al., 2003a) where an attempt to stabilise the ill-posed minimisation problem is described. A certain extension of the dimension of the input parameter vector entering the minimisation approach is examined in (Kathirgamanathan et al., 2003b). In the paper (Gab-Bock Lee et al., 2013) the measured air dose rates from the Fukushima accident are compared with the same values calculated by the optimised estimation using nonlinear minimisation. An extension of analysis on the measurement errors is given in Section 4.4.3. An extensive simulation experiment covers 1196 sets of the randomly perturbed measurements, each set for all 84 sensors on the terrain, is described in Section 4.4.4.

2. Prediction of random output fields using parametrised dispersion model SGPM

We have adopted a special modification of the dispersion model with the acronym SGPM based on the segmented Gaussian plume model. It can account approximately for dynamics of the released discharges synchronised with the short-term forecast of the hourly (half-hourly) changes of meteorological conditions. This model is able to describe the random nature of the problem and simulate the uncertainty propagation of the input model parameters. The distinction between variability and uncertainty of a certain input parameter is taken into account. Variability reflects changes of a certain quantity over time, over space or across individuals in population. Variability represents diversity or heterogeneity in a well-characterised population. The term “uncertainty” covers stochastic uncertainties, structural uncertainties representing partial ignorance or incomplete knowledge associated with the lack of perfect information about poorly-characterised phenomena or models, uncertain (ill-defined) release scenario or input model uncertainties. For purposes of the assimilation procedures, the sampling of fluctuations of input parameters repeatedly entering the SGPM model is internally driven by the algorithm for optimisation of the corresponding cost function.

In the following text, the upper case symbols are related to the random variables and lower case symbols stand for the actual values generated from the corresponding random distributions. The vector Θ of M random input model parameters θ_m can be schematically written as:

$$\Theta = [\theta_1, \theta_2, \dots, \theta_M]^T \quad (1)$$

Their specific realisations are generated with a corresponding sequence of random distributions D_1, D_2, \dots, D_M which are usually formulated on the basis of consensus among experts (range, type of distribution, and potential mutual dependencies). The model parameters usually have a physical meaning, such as the amount of discharged radioactivity, atmospheric stability characteristics, dispersion parameters, uncertainties related to dry and wet radioactivity fallout, wind field components, etc. The input parameters enter the SGPM model, which generates dispersion outputs submitted for further processing in the subsequent parts of the environmental model. Specifically in our case, the SGPM model is nested inside the environmental program system HARP (online access in (HARP, 2013)). The HARP system addresses all resulting meaningful output entities X_j being subject of interest, which can be formally collected into the output vector A with components X_j , $j = 1, \dots, J$. The multidimensional output $A(t)$ related to the time t

can be expressed according to the scheme:

$$\begin{aligned} \text{HARP}^{\text{SGPM}}(\Theta_1, \Theta_2, \dots, \Theta_M; t) &\Rightarrow \Lambda(t) \\ &= [\mathbf{X}_1(t), \mathbf{X}_2(t), \dots, \mathbf{X}_j(t), \dots, \mathbf{X}_J(t)]^T \end{aligned} \quad (2)$$

J is the total number of the resulting outputs. $\mathbf{X}_j(t)$ can be each of the conceivable examined entities, such as spatial fields of radioactivity deposited on the ground for each individual nuclide, doses and dose rates on the terrain from cloudshine, groundshine and inhalation, distribution of various ingestion doses in the later phase of an accident, etc. The symbol \Rightarrow expresses a nonlinear numerical procedure of the output generation. The random variable \mathbf{X}_j is represented as a discrete field of the respective entity j in each node i of the polar calculation grid. The computational polar grid around the potential source of pollution consists of 42 radial distances up to 100 km and 80 angle sectors. Then the dimension of the field \mathbf{X}_j is I , where $I = 42 \times 80 = 3320$ (number of the calculation nodes i of the polar grid). Due to their stochastic character, the true quantities of the output vectors

$$\mathbf{X}_j(t) = \mathbf{X}_j(\Theta_1, \Theta_2, \dots, \Theta_M; t) \quad (3)$$

are unobservable and can only be estimated using a probabilistic approach based on Monte-Carlo modelling. The sampling-based method consists of a successive multiple repetitive modelling of the output fields \mathbf{X}_j , always for each specific sample of the random input vector (1), specifically:

1. Generation of the particular n -th sample of the input vector $\theta^n = [\theta_1^n, \dots, \theta_m^n, \dots, \theta_M^n]^T$, where component θ_m^n stands for the n -th realisation of the m -th input random parameter Θ_m .
2. Propagation of the sample n through the model. It means substitution of θ^n into (2) and calculation of the corresponding n -th realisation \mathbf{x}_j^n of the random output entity \mathbf{X}_j as:

$$\text{HARP}^{\text{SGPM}}(\theta_1^n, \dots, \theta_m^n, \dots, \theta_M^n; t) \Rightarrow \mathbf{x}_j^n(t) \quad (4)$$

The adopted scheme of Monte-Carlo modelling uses the stratified sampling procedure LHS (Latin Hypercube Sampling) for generating the random samples. Common experience has shown that 1/3 iterations are typically required to get results equal to or better than the equivalent amount of crude Monte-Carlo iterations. Moreover, LHS avoids the extreme values and prevents the introduction of a bias provided the total number of simulation runs should be a multiple of the number of quantiles. LHS can produce good estimates of the mean and variance of the output distribution with significantly fewer simulations than a simple random sampling. The code HARP stands for an interactive subsystem for generating N LHS samples for various types of random distributions D_m of the components Θ_m for the vector of input parameters Θ . The resultant mapping of the pairs of vectors is arranged into the scheme:

$$\left\{ \mathbf{x}_j^n; \theta^n \right\}_{n=1, \dots, N} \quad (5)$$

where \mathbf{x}_j^n is a vector representing the particular n -th realisation (maybe imagined as a trajectory of pollution on the terrain) of the output entity \mathbf{X}_j relevant to the n -th realisation of input parameter vector $\theta^n = [\theta_1^n, \dots, \theta_m^n, \dots, \theta_M^n]^T$. The vector \mathbf{x}_j^n has the dimension $I = 3320$ corresponding to the extent of the computational polar grid. Provided that the value of the Monte-Carlo samples N is sufficiently high (~several thousand), the expression (5) provides the proper bases for:

- *Uncertainty analysis (UA)* – statistical processing of the pairs (5) can determine the extent of the uncertainty on predicted consequences and yield various statistics, such as sample mean and variance, percentiles of the uncertainty distribution on the quantity given, uncertainty factors, reference uncertainty coefficients, etc.
- *Sensitivity analysis (SA)* – identification of the model inputs that cause significant uncertainty in the output and/or screening of the model inputs that have negligible effect on the output with the aim to determine simplification and reduction of the computational burden. Various techniques for different measures of sensitivity are introduced (scatterplots, regression and correlation analysis, rank transformations, etc.).
- *Data assimilation (DA)* – provides data (5) for the trajectory simulations and estimation of the covariance structure of the model errors. The final goal is extraction of information from both the observations and prior knowledge to obtain reliable estimates.

For better understanding, let entity $j1$ stand for the radioactivity deposition of a certain radionuclide on terrain at time t . The discrete spatial distribution $\mathbf{x}_{j1}^n(t)$ can be visualised in 2-D as the particular n -th trajectory (trace) of the radioactive plume propagation. Similarly, the sum of cloudshine plus groundshine dose rates from a mixture of all discharged radionuclides (labelled, for example, as entity $j2$) forms the particular n -th trajectory $\mathbf{x}_{j2}^n(t)$ which can be directly confronted with the same type of the dose rate values incoming from the monitoring networks. Our experience was published in (Pecha et al., 2009).

3. Data assimilation – a way from model to realistic predictions

The mathematical model remains only a simplification of the complex physical phenomena, and a significant extent of the uncertainties involved can degrade credibility of the model predictions. Our models merely approximate the complicated real situation during an accidental radioactive release. The simplifications occur on levels of both conceptual and computational model selections. Nevertheless, experience accumulated with respect to physical models of pollution propagation through the living environment provides us with valuable prior knowledge. Stochastic character of the task calls for introduction of assimilation techniques, which ensure improvement of the model towards reality. From a general view on assimilation, the data assimilation procedures should accomplish an optimal blending of all information resources, including prior physical knowledge given by the model, observations incoming from the terrain, past experience, expert judgment, and possibly also intuition (Talagrand, 1997; Kalnay, 2006). Merging of all of these contending resources for purposes of improving our predictions is a principle of the DA. The assimilation to observation algorithm lead to a generalised least-squares approach minimising a measure (proper cost function) of difference between the available information and the system state. Either advanced statistical assimilation procedures or a simpler optimisation approach described here can be classified such as the methods for solving the inverse problem.

According to the DA methodology, the general state-space formulation in the continuous time domain is in practice substituted by filtering in discrete time. Consequently, we consider the time evolution of the states as a sequence $\{\mathbf{X}_k\}_{k=1, \dots, K}$. The true unobservable vector \mathbf{X}_k related to the time $t = t_k$ is given by (3) where the index j is, for simplicity, omitted. We assume that the R -dimensional vector of measurements \mathbf{y}_k is obtained during the time interval $\langle t_{k-1}; t_k \rangle$. The proposed analysis takes into account errors

of both the model predictions and the real observations from terrain (Kalnay, 2006; Ristic et al., 2004). Specifically, we treat these errors as mutually uncorrelated. Let there be R receptor points on the terrain where the respective output values are measured. The formulation in the discrete time domain assumes the observation vector:

$$\mathbf{y}_k \equiv [y_k^1, y_k^2, \dots, y_k^R]^T \quad (6)$$

where values y_k^r are the measurements at points r in the time interval $\langle t_{k-1}, t_k \rangle$. Generally, the number of receptors is much lower than the number of the calculation nodes I and we encounter a problem with rare measurements. Positions of the sensors generally differ from the points of the calculation grid. We shall use terminology from data assimilation and introduce the observation operator H , especially its linear observation matrix H . H is an $R \times I$ matrix that transforms vectors \mathbf{x}_k from the model space (having length I) into the corresponding vector $\tilde{\mathbf{x}}_k$ in the observation space (having length R) according to the matrix notation

$$\tilde{\mathbf{x}}_k = H \cdot \mathbf{x}_k \quad (7)$$

Components \tilde{x}_k^r of the vector $\tilde{\mathbf{x}}_k$ represent the model predictions interpolated at the positions of observations $r = 1, \dots, R$.

3.1. Advanced statistical formulation of the general assimilation problem

The problem of data assimilation can be approached by either variational or sequential algorithms. The variational methods seek the initial condition such that the forecast best fits the observations. The advanced representative in the field, the 4D-Var variational inverse modelling technique, searches for the initial conditions of a model such as to minimise a scalar quantity, known as the cost or penalty function. While the variational techniques proceed by the global fitting of an assimilating model to the available information, the sequential assimilation (filtering) involves a statistical minimum mean squares error estimation approach. The sequential methods use a probabilistic framework and give estimates of the whole system state sequentially by propagating information forward in time.

The analytical form of the posterior density is intractable and obtaining an exact solution from it is often difficult or impossible. Instead of solving the Bayesian recursive filter analytically, the posterior probabilities are substituted by a set of randomly chosen weighted samples (trajectories). Several alternative modifications of the Monte-Carlo methods were introduced for sampling from the posterior distributions of the system state. An overview of the proper Monte Carlo methods is given in (Andrieu et al., 2010). The sequential Monte-Carlo (SMC) and Markov-Chain Monte-Carlo (MCMC) methods proved to be efficient tools for sampling from high-dimensional probability distributions for non-Gaussian and nonlinear models. These algorithms facilitate sequential approximation of posterior probability densities and marginal likelihoods sequences, thus enabling inference in the state-space models.

The popular particle filtering (PF) – also known as sequential Monte Carlo – generates samples from the current state trajectory (“particles”) and uses the re-sampling procedure to prevent the sample impoverishment problem (e.g., Doucet et al., 2001; Kalnay, 2006; Andrieu et al., 2010; Ristic et al., 2004). This approach has been used in Šmídl et al., 2009a) and Hofman et al., 2009 for Gaussian puff models. The capability of the segmented Gaussian plume model SGPM to effectively generate the multiple random realisations (trajectories) was verified (Pecha et al., 2009, Hofman and Pecha, 2011). Application of the PF technique to examination

of detection abilities of the monitoring networks using multiple assessment criteria is treated in (Šmídl et al., 2014).

3.2. Nonlinear regression analysis as a tool for integration of observations with the model predictions

The maximum likelihood approach is often used as a computationally efficient first approximation of the full Bayesian treatment of the problem (Šmídl and Hofman, 2014). The assimilation techniques can be classified either as a non-parametric approach, where large spatial fields are processed and adjusted, or as a parametric access (Winiarek et al., 2011). We follow the parametric approach and optimise the selected model parameters in order to reach the best correspondence of the model prediction to the observations measured in the terrain. The implied maximisation/minimisation problem is complicated by the fact that the parametric segmented Gaussian plume model SGPM (2) is nonlinear.

The model SGPM provides generation of the n -th sample of the background vector \mathbf{x}_k belonging to a certain set of input parameters $(\theta_1^n, \dots, \theta_m^n, \dots, \theta_M^n)$ according to scheme (4); these parameters are modified for the discrete time domain k as:

$$\text{HARP}^{\text{SGPM}}(\theta_1^n, \dots, \theta_m^n, \dots, \theta_M^n; k) \Rightarrow \mathbf{x}_k^n \quad (8)$$

The probabilistic version of the SGPM algorithm is adapted for the minimisation procedures. The procedure BCPOL from the IMSL library is initially tested; in each iterative step p it internally provides a new set of the minimisation parameters $(\theta_1^p, \dots, \theta_m^p, \dots, \theta_M^p)$, which are passed through the SGPM model to the enumeration (9). The previous scheme (8) is formally rewritten as:

$$\text{HARP}^{\text{SGPM}}(\theta_1^p, \dots, \theta_m^p, \dots, \theta_M^p; k) \Rightarrow \mathbf{x}_k^p \quad (9)$$

Number M of the input parameters is rather high (up to several tenths) and for practical purposes only S of them are treated as random. The rest of them are deemed fixed and represented by their best estimated values labelled by the index *best*. The input parameter vector (1) is then split to:

$$\Theta \equiv [\Theta_1, \Theta_2, \dots, \Theta_S, \theta_{S+1}^{\text{best}}, \dots, \theta_M^{\text{best}}]^T \quad (10)$$

In other words, a certain number S of selected problem-dependent optimisation parameters $\Theta_1, \Theta_2, \dots, \Theta_S$ are then considered to be uncertain and subject to fluctuations within a specific range. In the next step, a loss function F is constructed using the assumption of the Gaussian-distributed measurement errors as a sum of squares differences at the measurement points between the values of model predictions and values observed in terrain:

$$F(\theta_1^p, \dots, \theta_S^p; k) = \sum_{r=1}^{r=R} (\tilde{\mathbf{x}}_k^r(\theta_1^p, \dots, \theta_S^p) - y_k^r)^2 \quad (11)$$

$\tilde{\mathbf{x}}_k^r, r = 1, \dots, R$ are components of the vector of model predictions transformed by Equation (7) into the observation space. The chosen minimisation algorithm searches for a minimum of the scalar function F of S parameters $(\theta_1, \dots, \theta_S)$ starting at an initial “best estimate”. At a glance, the test points $(\theta_1, \theta_2, \dots, \theta_S)$ of the objective function F are arranged as an S -dimensional simplex, and the algorithm tries to iteratively replace individual points with an aim of shrinking the simplex towards the best points. The minimisation algorithm controls the procedure until the best fit of modified surface with observation values is reached. The procedure continues for the next time domain $k + 1, \dots, K$. An important feature of the method is the preservation of physical knowledge, because the new set of parameters $(\theta_1^{p+1}, \theta_2^{p+1}, \dots, \theta_S^{p+1})$ evaluated by the

minimisation algorithm always re-enters the entire nonlinear environmental model HARP^{SGPM} according to Equation (9).

The commonly used Nelder-Mead (NM) simplex method of heuristic direct search minimisation was tested for some basic scenarios of accidental harmful discharges. The objective multidimensional function F of S variables given by (11) subjected to bounds is minimised starting at the initial best guess $F(\theta_1^{best}, \dots, \theta_S^{best})$. The constraints are put on the lower and upper bounds of each parameter $\theta_s, s=1, \dots, S$ in the form:

$$\theta_s^{best} - b_s^{low} \leq \theta_s \leq \theta_s^{best} + b_s^{upp} \quad (12)$$

Indices *low* and *upp* stand for lower and upper margins for the allowed values of the parameter θ_s . The Nelder-Mead method turned out to be appropriate for analyses of the radioactive plume propagation when extra high accuracy of the solution is not required. It is relatively insensitive to the numerical noise and the results are comparable with other non-derivative minimisation methods. Slow asymptotic convergence sometimes occurs for the NM method. A problem of size limitations exists, and the method is predestined for a small number of parameters – our experience is summarised in (Pecha and Hofman, 2008). The problem can arise when evident parameter correlations occur. Only the ratio and not their individual values can be determined then.

4. Numerical experiment on minimisation approach

4.1. Setup of TWIN experiment

The following numerical experiments are conducted as a TWIN experiment. Simulation of the missing real measurements should be performed due to the lack of proper real data. Several reasonable methods for the TWIN data generation were adopted. The same dispersion model is used for generating the TWIN data. In order to avoid an “identical” experiment, the raw TWIN data can be somewhat perturbed. We shall introduce certain dissimilarities by using different meteorological forecasts in the TWIN model and the model predictions. The “artificial” measurements are generated just at the positions of the sensors in the monitoring network. The synthetic measurements play the role of a reference plume or trace on the terrain. The assimilation technique optimises the model parameters on the basis of optimal blending between the reference true plume (or trace) and the reconstructed (assimilated) values. The idea of artificial measurements has its own practical implication when a wide range of various measurement noise perturbations can be tested (Section 4.4.4).

4.2. Earlier experience: one-stroke optimal blending of model predictions with measurements

Recent preliminary examinations try to extend the number of relevant input model parameters entering the minimisation. In (Kathirgamanathan et al., 2003b) uncertain source height, lateral eddy diffusivity and source distance from measuring points are also considered in addition to the source rate. Similar examinations of the nonlinear Nelder-Mead (NM) minimisation treating a capability to manage a higher number of relevant input parameters were discussed in (Pecha and Hofman, 2008). The NM procedure is applied to a simple radioactive release scenario of an accidental one-hour hypothetical release of the radionuclide ¹³¹I discharged from a nuclear facility into the atmosphere. Model predictions of the radioactivity deposition of ¹³¹I are interpreted as a Gaussian surface (or a superposition of partial Gaussian extents) over the terrain. The values of the deposition are related to the time shift from release beginning T^{start} up to the time T^{end} , when the

radioactive cloud has just left the monitoring area. It means we have examined only one time domain $\langle T^{start}; T^{end} \rangle$. The measurements are assumed to be related to T^{end} . The objective is to take into account both model predictions related to T^{end} and available rare measurements incoming from the terrain and simply improve the predictions of the spatial distribution of the deposited radioactivity. We shall use the term one-stroke corrections (unlike the stepwise recursive corrections described below in Section 4.4). The one-stroke iterative process of NM minimisation of the function F proceeds according to equation (11) for $k = K = 1$. It consists of consecutive adjustments of the resulting response surface, always according to the new evaluation of the parameters in the p -th minimisation step $(\theta_1^p, \theta_2^p, \dots, \theta_S^p)$, expressed specifically by the associated vector of the dimensionless factors $[c_1, c_2, c_3, c_4]^T$ (see Table 1). We provide more details online in (Pecha, 2008).

4.3. Prediction of the dose rate propagation in the early stage of a radiation accident

From a perspective of examining the monitoring network capabilities, the principal significance belongs to the output entity of the external irradiation expressed by the ground level dose rates. It consists of a sum of cloudshine and groundshine fields. The environmental code HARP with its dispersion model based on segmented Gaussian plume model (SGPM) was designed to be fast enough for its deployment in the sequential DA procedures. More detailed information is available online (HARP, 2011).

Radioactive substances can be discharged into the atmosphere with a large nuclide variability and steep time changes. The multi-segment and multi-nuclide universal algorithm has been developed to determine the spatial and temporal fields of dose rates. The real release time dynamics is partitioned into a number of fictitious one-hour consecutive segments *seg*, $seg = 1, \dots, SEG$, each with an equivalent value of the homogenous averaged radioactivity release source strength q_{seg} [$\text{Bq}\cdot\text{s}^{-1}$]. The corresponding hourly discharge is labelled as Q_{seg} [$\text{Bq}\cdot\text{hour}^{-1}$], $Q_{seg} = q_{seg} \times 3600$. The maximum permissible number of *SEG* is 72, hence releases with a duration of up to 3 days can be analysed. Synchronisation with an hourly forecast of meteorological conditions is performed. The segment *seg* is released from the source of pollution just at hour *seg* from the beginning identical to that of the accident. Each hourly segment *seg* is modelled in its all consecutive hourly meteorological phases *met* (more specifically, it is labelled as *met(seg)*) relative to the initial discharge of the segment *seg* ($met = 1, \dots, MET(seg)$). The value of $MET(seg)$ is determined dynamically as the final relative hour when the partial plume *seg* leaves the monitoring area (100-km vicinity around the source of pollution). The hourly segment *seg* of the release is spread during the first hour as a straight-line Gaussian plume driven by the meteorological forecast for $met(seg) = 1$. In the following hours, the segment *seg* spreads according to the available hourly meteorological forecast for the successive relevant meteorological phases *met* ($met = 2, \dots, MET(seg)$). Here the segment *seg* is treated as a “prolonged puff” and its dispersion and depletion (due to radioactive decay and wet or dry fallout) during the movement is simulated numerically by means of a large number of elemental shifts. A more detailed description of the procedure can be found on the web (HARP, 2011).

The external irradiation from the cloud and from radioactivity deposited on the terrain is considered. Let us consider propagation of one-hour homogenous segments *seg*. The output fields of the cloudshine and groundshine dose rates $RATE_{cloud}^{nuc}(i; seg, met)$ and $RATE_{ground}^{nuc}(i; seg, met)$ (both in mSv/hour) in discrete computation nodes *i* always belong to a single pair (*met, seg*). Both values are easily determined from the pre-calculated basic dispersion values. The location on the terrain is expressed in discrete representations

Table 1

Choice of NM algorithm bounds for four important input model parameters.

Parameter	unit	Used inside code	NM bounds
θ_1 : source release rate	[Bq s ⁻¹]	$q = c_1 \times q^{\text{best}}$	$c_1 \in (0.1; 2.9)$
θ_2 : horizontal dispersion σ_y	[m]	$\sigma_y(x) = c_2 \times \sigma_y(x)^{\text{best}}$	$c_2 \in (0.1; 3.1)$
θ_3 : wind direction φ	[rad]	$\varphi = \varphi^{\text{best}} + c_3 \times 2\pi/80$	$c_3 \in (-5.0; 5.0)$
θ_4 : dry depos. velocity vg	[m s ⁻¹]	$vg = c_4 \times vg^{\text{best}}$	$c_4 \in (0.1; 4.0)$

of the nodes i of the computational polar grid. The resulting values are evaluated using superpositions of relevant sequences for each result (seg, met) , i.e., $(seg, met(seg))$.

Cloudshine: Distribution of the cloudshine dose rates $RATE_{cloud}$ on the terrain pertaining to the time interval from the beginning of the release up to the hour T are computed as a superposition of contributions from all hourly segments (seg, met) that are at the time T still drifting over the terrain. These relevant segments are chosen and summed up according to their equality $seg + met - 1 = T$.

$$RATE_{cloud}^{nuc}(i; T) = \sum_{seg=1}^{seg=SEG} \times \sum_{met=1}^{met=MET(seg)} \{RATE_{cloud}^{nuc}(i; seg, met)\}_{seg+met-1=T} \quad (13)$$

The total dose rate from irradiation from the radioactive cloud from all released nuclides is given by:

$$RATE_{cloud}(i; T) = \sum_{(nuc)} RATE_{cloud}^{nuc}(i; T) \quad (14)$$

Determination of the total cloudshine doses [mSv/T] accumulated at location i during the progression of the one-hour segment seg in all its meteorological phases met , $met = 1, 2, \dots, MET(seg)$ should reflect the irradiation doses from the radioactive cloud accumulated in the nodes i on the terrain during the whole interval of the plume propagation $< 0; T >$. It is computed as a superposition of contributions from all hourly segments (seg, met) that are now (and have been) drifting over the terrain during $< 0; T >$. These relevant segments are chosen and summed up according to the inequality $seg + met - 1 \leq T$.

$$DOSE_{cloud}^{nuc}(i; T) = \sum_{seg=1}^{seg=SEG} \times \sum_{met=1}^{met=MET(seg)} \{RATE_{cloud}^{nuc}(i; seg, met)\}_{seg+met-1 \leq T} \quad (15)$$

or alternatively:

$$DOSE_{cloud}^{nuc}(i; T) = \sum_{t=1}^{t=T} RATE_{cloud}^{nuc}(i; t) \quad (16)$$

The total irradiation dose from all nuclides in the cloud is given by superposition:

$$DOSE_{cloud}(i; T) = \sum_{(nuc)} DOSE_{cloud}^{nuc}(i; T) \quad (17)$$

Groundshine: The groundshine dose rates and irradiation doses should be taken as sums of contributions from the deposited radioactivity during the whole trajectory of the segments. For a

given hour T the specific released segment seg goes through its meteorological phases $met(seg) = \{1, \dots, T-seg\}$. We have to account for the contributions modified by radioactive decay from the radioactivity deposited in the previous met phases according to:

$$RATE_{ground}^{nuc}(i; T) = \sum_{seg=1}^{seg=T} \left\{ \sum_{met(seg)=1}^{met(seg)=T-seg} RATE_{ground}^{nuc}(i; seg, met(seg)) \times \exp[-\lambda_{nuc} \cdot (T - seg - met(seg) + 1)] \cdot 3600 \right\} \quad (18)$$

The values $RATE_{ground}^{nuc}(i; seg, met(seg))$ are again determined from the pre-calculated basic dispersion values, each nuclide has decay constant λ_{nuc} [s⁻¹]. The total groundshine dose rates from all released nuclides nuc are given by:

$$RATE_{ground}(i; T) = \sum_{(nuc)} RATE_{ground}^{nuc}(i; T) \quad (19)$$

The doses of irradiation from deposited radioactivity $DOSE_{ground}(i; T)$ in [mSv/T], which are accumulated at location i , are expressed as sums of effects in each hour of the plume propagation:

$$DOSE_{ground}(i; T) = \sum_{(nuc)} \sum_{t=1}^{t=T} RATE_{ground}^{nuc}(i; t); \quad (20)$$

External irradiation effect: In the following analysis, we shall focus on evolution of the distribution of the dose rate values induced by the external irradiation according to the sum:

$$D(i; T) = RATE_{cloud}(i; T) + RATE_{ground}(i; T) \quad (21)$$

It denotes the total dose rate [mSv h⁻¹] at location coordinates i just at hour T after the release start. These external irradiation rates interpolated to the positions of measurement points can be directly compared with observations (6) incoming from the terrain.

Note: The apparent complexity can prevent us from clearly understanding of the advantage of the presented method of segmentation. Its main benefit is the possibility to effectively simulate the stepwise evolution of contamination in the early stage of a radiation accident. It facilitates an implementation of recursive model parameter re-estimation and radioactive plume tracking. The trick of our approach lies in the separation of the calculation into two steps. In the first step, the time-consuming dispersion calculations of the main four basic radiological quantities are determined and archived, namely near-ground activity concentration in air, time integral of near-ground activity concentration in air, radioactivity deposited on terrain, and time integral of the deposited radioactivity. These quantities are expressed in the above-described segmented representation as the spatial fields for each $(seg, met(seg))$. On the basis of these values, the overall estimation of the radiological consequences is carried out in the second step. Practically any kind of potentially possible huge radiological outputs (many hundreds, including those denoted by $RATE_{cloud}$, $RATE_{ground}$, etc. above), can easily and quickly be generated with the

aid of a simple multiplication by the constants comprising the corresponding dose conversion factors. The processing of the second step is facilitated using the effective visualisation subsystem (HARP, 2013).

4.4. Recursive inverse modelling scheme in the early stage of accident using an optimisation approach

As mentioned in the beginning of Section 3, the main objective of the dispersion calculation is description of the time evolution of the system state in the discrete consecutive time domains k as a sequence $\{\mathbf{x}_k\}_{k=1,\dots,K}$. Unlike the one-stroke approach described in Section 4.2, the process is now conducted recursively. In each time step, the resulting outputs from the previous step $k-1$ are predicted forward using expressions (8) and NM minimisation (11) to the next k , taking into account the observations (6) incoming from the real Early Warning Network (see Fig. 3). There are many model parameters that influence the shape of the plume: release source strength of radioactivity q_k [Bq.s⁻¹], release height, category of atmospheric stability, height of the mixing layer, terrain parameters, etc. As described in Sec. 4.2, four model parameters have been selected for one-stroke correction of the radioactive deposition trace on terrain related to the time when the plume just left the terrain. In this Section, we are solving a much more complicated task of the near-field dispersion problem consisting in sequential stepwise assimilation of the principal model parameters using observations. A special task of the recursive plume tracking in its individual consecutive hours of propagation and parameter re-estimation is handled. In each time step with a one-hour duration, the corrections of the model with the measurements incoming during this time step are carried out. The notation from Section 4.2 is retained.

4.4.1. Setup of the numerical experiment

The main three model parameters governing the specific capacity of the plume radioactivity and transport are selected. Within the SGPM concept of the release segmentation all three parameters are assumed to be constant in each one-hour interval k . We consider the source strength q_k [Bq.s⁻¹] of radioactivity discharge, and furthermore we shall calibrate the wind direction and wind speed in the particular time steps of one hour in duration using the additive offset c_φ and multiplicative offset c_{u10} , respectively, according to Table 2. All other parameters are given by their best estimated deterministic values. The regular weather conditions are supposed to be known from the numerical weather prediction. The composition of the discharged radionuclides in the release is assumed to be known including their physical-chemical form governing the intensity of wet and dry fallout on the terrain.

Recursive stepwise assimilation scheme at near distances from the source of pollution is applied to one-hour hypothetical release of radionuclides with the best estimated (nominal) hourly discharges Q_j^{best} [Bq.hour⁻¹] estimated ad hoc as:

$$\begin{matrix} \text{KR88} & 1.00\text{E}17 \\ \text{I131} & 1.00\text{E}15 \\ \text{CS137} & 1.00\text{E}15 \end{matrix} \quad (22)$$

Note: One should exhaust all available additional information in order to improve the predictions of the radiological consequences (see the “golden rule” of assimilation in Section 4.4.2). Provided that there is a certain remaining time in the pre-release phase of an accident, the emergency management staff can launch fault tree analysis (deductive failure analysis) in which an undesired state of the system is analysed using Boolean logic to combine a series of lower-level events. Time dynamics of the radioactive release episodes shows a specific behaviour of the particular nuclide groups: noble gases (Kr, Xe), halogens (Br, I), alkali metals (Rb, Cs), tellurium group (Se, Sb, Te), alkaline earth (Ba, Sr), noble metals (Ru, Rh, Pd, Co), lanthanides Known burnup level provides the sufficient estimation of the actual core inventory and the ad hoc scheme (22) can now be replaced with a more qualified guess based on the nuclide group discharges defined by an expert.

After the first hour the release is assumed to stop. The further propagation of this single cloud is modelled in all consecutive hours. The meteorological forecast from Sept. 3, 2009 was selected. A simple forecast for the point of release (format FECZ) is shown in Table 3. The time stamp of 20090903–23 defines the release start on Sept. 3, 2009 at 23.00 p.m. The file is used for generating the TWIN set of artificial measurements. The associated more detailed meteorological data (format HIRL) on the grid 200 × 200 km around the source of pollution also enters the calculation. Specifically, the gridded meteorological data HIRL with a time stamp of 20090903–2300.txt controls the progression of the radioactivity transport whenever the dispersion model is called. The TWIN model is constructed with help of selected fixed quantities. Specifically, for the release rate in the first hour $k = 1$, the fixed chosen value $c_q^{TWIN} = 7.77$ is substituted into $q_1^{TWIN} = c_q^{TWIN} \cdot q_1^{best}$. In order to avoid an identical experiment, two different meteorological models are simultaneously used. The TWIN model uses simple meteorological forecast FECZ for each hour in the point of release (Table 3) which is applied at once in the whole analysed region (time-dependant, spatially-constant). On the other hand, during multiple calls of the minimisation procedure, the model predictions (8) take out gridded meteorological forecast HIRL (time-dependant, spatially-dependant mode). Detailed instructions how to create the TWIN experiment are provided in (ASIM, 2013) for those users who have no better alternative to obtain more realistic observations.

The numerical computational procedure for calculation of the effective dose rate quantities from the external irradiation is formulated in Section 4.3. Within the time step k the sum (21) of quantities $RATE_{cloud} + RATE_{ground}$ is assumed to be homogenous according to expressions (13) to (20). The 2-D trajectories of the dose rate just at the moment after 3 and 8 h from the release beginning are illustrated in Fig. 1. The visualisation belongs to the best estimated values Q_j^{best} , given (22). The gridded HIRL forecast

Table 2
Parameter decomposition and bounds for the near-field recursive tracking of the plume.

Parameter	unit	Representation inside code	NM bounds
θ_1 : source release rate q	[Bq s ⁻¹]	$q = c_q \times q_1^{best}$ ^b	$c_q \in \langle 0.1; 10.0 \rangle$
θ_2 : wind direction φ	[rad]	$\varphi = \varphi^{best} + c_\varphi$	$c_\varphi \in \langle -90.0^\circ; +90.0^\circ \rangle^a$
θ_3 : wind velocity at 10 m height u_{10}	[m s ⁻¹]	$u_{10} = c_{u10} \times u_{10}^{best}$	$c_{u10} \in \langle 0.1; 4.0 \rangle$

^a Degrees from φ^{best} ; +/–: clockwise/counter clockwise.

^b c_q is the same for all nuclides nuc in discharge, more precise discrimination c_q^{nuc} is not so far practicable.

Table 3
Hourly weather forecast in format FECZ for the point of release at 20090903–2300.

Hour of release	Wind direct. (deg) ^a	Wind speed (m/s)	Pasquill categ. of stability	Precipitation (mm/h)
1	270.00	2.30	E	0.00
2	238.00	2.70	D	0.00
3	230.00	2.10	D	0.00
4	224.00	1.50	D	0.00
5	225.00	1.10	D	0.00
6	195.00	1.10	D	0.00
7	185.00	1.50	D	0.00
8	188.00	2.50	D	0.57
9	184.00	2.70	D	0.89
...

^a wherefrom blows: degees from north, clockwise.

provides the values $\varphi^{best}(x,y;k)$, $u_{10}^{best}(x,y;k)$, ($k = 1, \dots, 8$ h).

The TWIN trajectories are supposed to be driven by the point meteorological data in format FECZ shown in Table 3 according to the chosen fixed TWIN values $\varphi^{TWIN}(x = 0, y = 0; k)$, $u_{10}^{TWIN}(x = 0, y = 0; k)$, $k = 1, \dots, 8$ h. Concurrently, the radioactivity release lasts only within the first hour $k = 1$, $Q_{k=1}^{TWIN} = Q_1^{best}$, c_q^{TWIN} (see next). The trajectories just after 3 and 8 h of the plume propagation are depicted in Fig. 2. Both formats HIRL and FECZ are mutually conjugated through a given identical time stamp. This fact could still introduce a demonstrable resemblance between the results generated with the aid of HIRL and FECZ. In order to avoid the “identical” experiment, the additional raw TWIN data modifications are introduced. Whilst the model starts the calculations with gridded meteorological data at 20090903 4–2300, the TWIN calculations using FECZ format starts one hour forward (hence the first row in Table 3 is skipped). As mentioned above the fixed value $c_q^{TWIN} = 7.77$ is substituted into $q_1^{TWIN} = c_q^{TWIN} \cdot q_1^{best}$. The recursive forcing of the model predictions towards the measurements represented by the TWIN model will be demonstrated. We shall examine the source term’s ability of re-estimation expressed by convergence $c_q^{asim} \Rightarrow c_q^{TWIN}$ when the initial guess for the first

iteration p of the NM minimisation is given by substitution of the best estimated model parameter values into the environmental model (4).

The details of the simulation experiment are given in Appendix A. The index p stands for p -th iteration of the non-linear minimisation of the Nelder-Mead (NM) algorithm, $P_{max}(k)$ denotes the index when the convergence in the time step k was reached. Specifically, the resulted assimilated parameters:

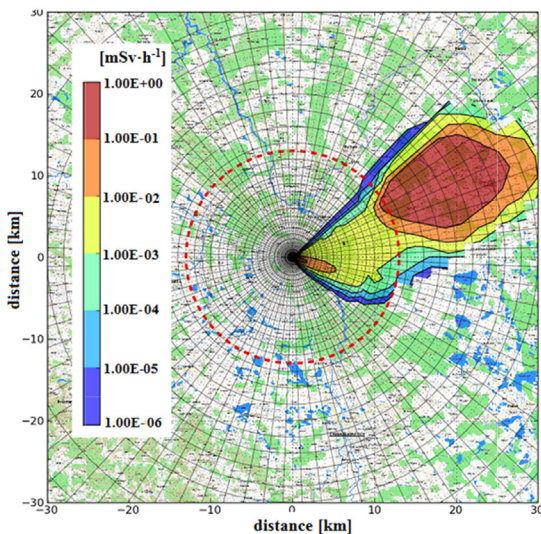
$$c_q^{asim}(k = 1), c_\varphi^{asim}(k), c_{u10}^{asim}(k) \quad (23)$$

in each individual recursive time steps (hours) k are expected to converge to the chosen fixed TWIN values:

$$c_q^{TWIN}(k = 1), c_\varphi^{TWIN}(k), c_{u10}^{TWIN}(k) \quad (24)$$

in the course of $P_{max}(k)$ iterations of the NM algorithm. The convergence is driven through the evaluation of the scalar function F from Equation (11). For the final stage at 8 h after the release start, the “best” trajectory after the blending with incoming observations is step by step inclined to the TWIN shape and magnitudes.

Model: Best Estimate - Effective external dose rate just after $k=3$ hours from the release start [$\text{mSv}\cdot\text{h}^{-1}$]



Model: Best Estimate - Effective external dose rate just after $k=8$ hours from the release start [$\text{mSv}\cdot\text{h}^{-1}$]

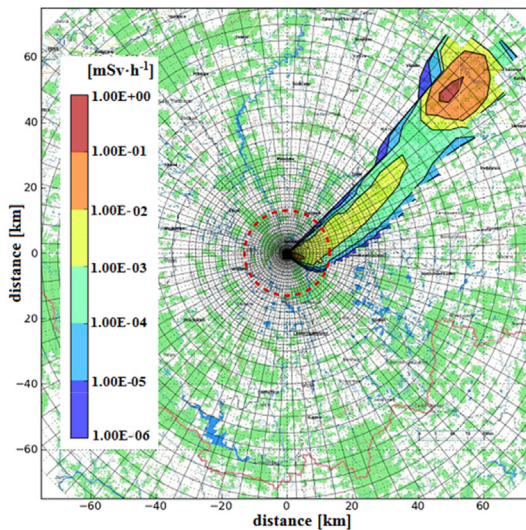


Fig. 1. Model predictions with the best estimated values of the input model parameters. The plume propagation is driven by the fine-gridded meteorological forecast in the format HIRL.

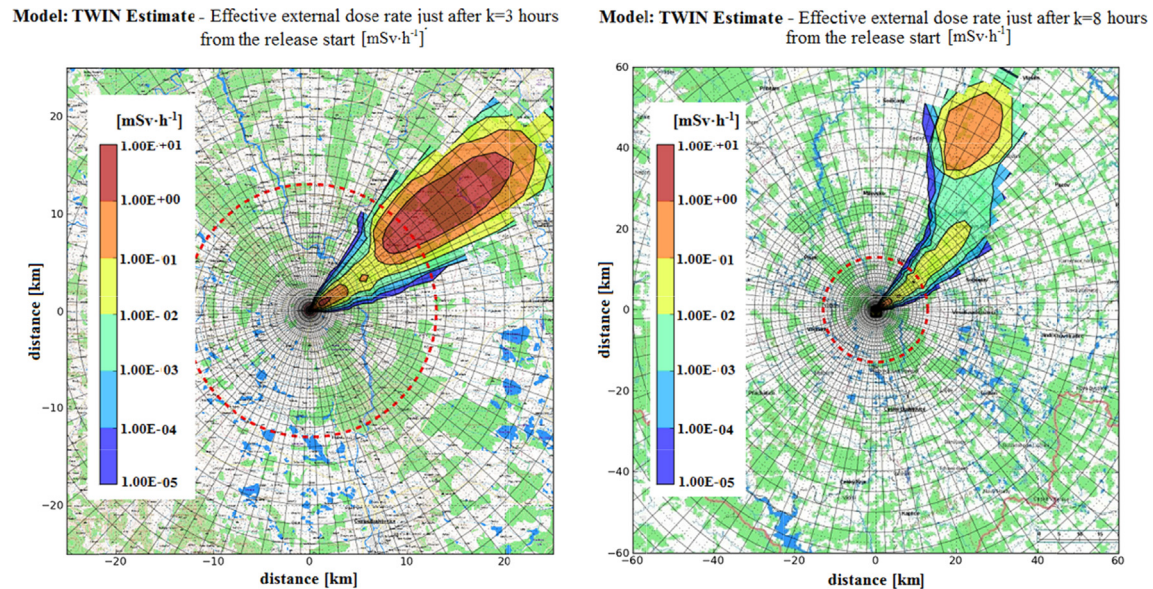


Fig. 2. TWIN trajectories (chosen fixed value $c_q^{TWIN} = 7.77$) driven by weather forecast FECZ for a single point of release according to Table 3 where the first row is skipped (shift one hour forward).

4.4.2. Progression of the plume recursive tracking in the successive time steps

The recursive process in the first three hours will be illustrated in Figures below. The plume travels over the area of the emergency planning zone (~16 km), where is more or less sufficient coverage by sensors of the real EWN (Early Warning Network) of NPP Temelin. The EWN can be exploited for purposes of the following data assimilation procedure.

Within the assimilation procedure the model predictions are step by step forced to the TWIN shape and magnitudes. No problems with convergence of the NM minimisation algorithm have been encountered for this basic scenario. Robustness and somewhat inflexible general approach of the basic direct search NM algorithm are mentioned in Appendix B. The method has been proven to have very good applicability in the case of sensitivity analysis to noisy measurements presented in Section 4.4.3, which follows. So far, no extra effort has been given to analysis of outlying situations where the inversion could fail: for example, because of too poor observability.

Two specific features for the segment in the first hour of its propagation should be pointed out:

- The main part of EWN is a teledosimetric system (TDS) consisting of two circles. The inner circle is positioned on the NPP-fence (see Fig. 3) and consists of 24 stations 2.5m above ground. The outer II circle incorporates 52 measurement positions located at larger distances, mainly in the emergency zone or its near vicinity. This net is additionally supplemented by several mobile stations appropriately located in medium distances. A relatively dense net of teledosimetric sensors in the TDS ring enables us to sufficiently estimate the multiplicative factor c_q for the source strength re-estimation.
- The source strength and mean advection velocity of the plume incorporate strong mutual dependency when calculating the dose rate values. For this reason we shall follow the “golden rule” of assimilation: “All available information resources should be taken into account”. Up to now we have omitted the available

real onsite meteorological measurements for the time of release. Now we are reassigning the best estimated value u_{10}^{best} (when calculating the model prediction using HIRL meteo format) by the measured value u_{10}^{tower} from onsite meteorological tower measurement which is assumed to be fixed and constant during all minimisation iterations for the first hour (see “Constraints” in Scheme in Appendix A).

Some results produced within the course of the assimilation procedure in the first hour of propagation $k = 1$ are illustrated in Fig. 4. Its left part stands for the initial guess trajectory of the NM algorithm which belongs to the best estimate of all input parameters with the exception of the wind direction and velocity, which are reassigned by measurements from meteorological tower in the release point. The real measurements $u_{10}^{tower}(k = 1) = 2.7 \text{ m} \cdot \text{s}^{-1}$ and averaged $\varphi^{tower}(k = 1) = 285.8^\circ$ were found and substituted in the original gridded prediction set. The initial guess enters the direct search algorithm which step by step inclines to the selected TWIN “measurements” represented by options $c_q = 7.77$ (test for the source term re-estimation); $c_\varphi = -46.90^\circ$ (from the 2nd row in Table 3); $c_{u10} = 1.00$. The NM minimisation starts from the best estimate trajectory (Fig. 4, left) with constraints in each iteration step p (see Appendix A). As follows from the above discussion, a very tight constraint should be imposed on $u_{10}(k = 1)$. The convergence was reached after 124 iterations and the relevant assimilated trajectory (Fig. 4, right) is very close to the prescribed TWIN “measurements” for $k = 1$.

The superposition of the second hour variations on the previous fixed assimilated trajectory for the first hour is shown in Fig. 5. The left-hand part stands for the first guess in the second hour, which means the assimilated trajectory from the previous first hour $k = 1$ (Fig. 4, Right) plus the best estimate of the segment in the 2nd hour (constructed from the parameters $c_\varphi^{best}(k = 2)$, $c_{u10}^{best}(k = 2)$ given by the meteorological format HIRL for the centre of the nominal plume segment in the second phase).

The following Fig. 6 presents the minimisation cycle for the third hour. The first guess (Fig. 6, left) consists of the previous, already

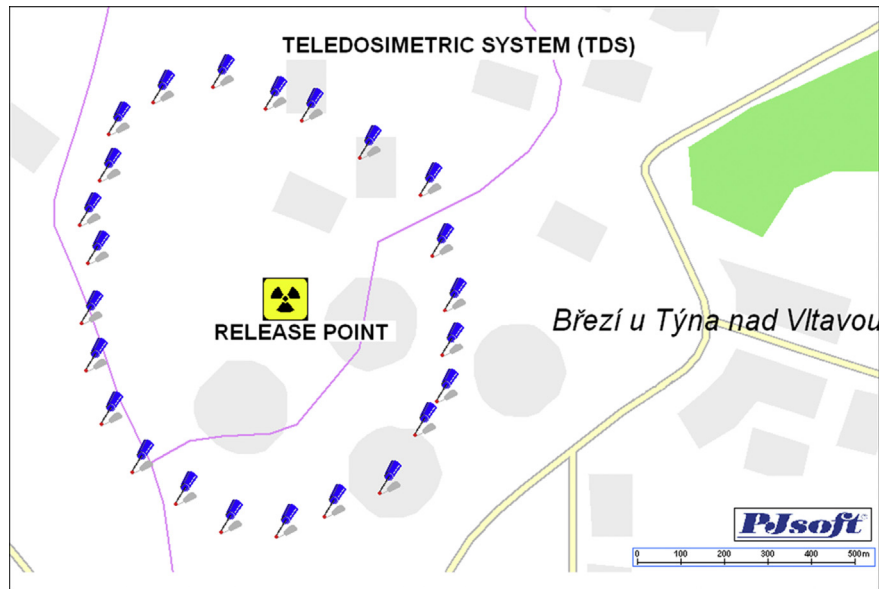


Fig. 3. TDS on fence of NPP Temelin – 24 detectors. Additional 52 measurement positions are located at larger distances.

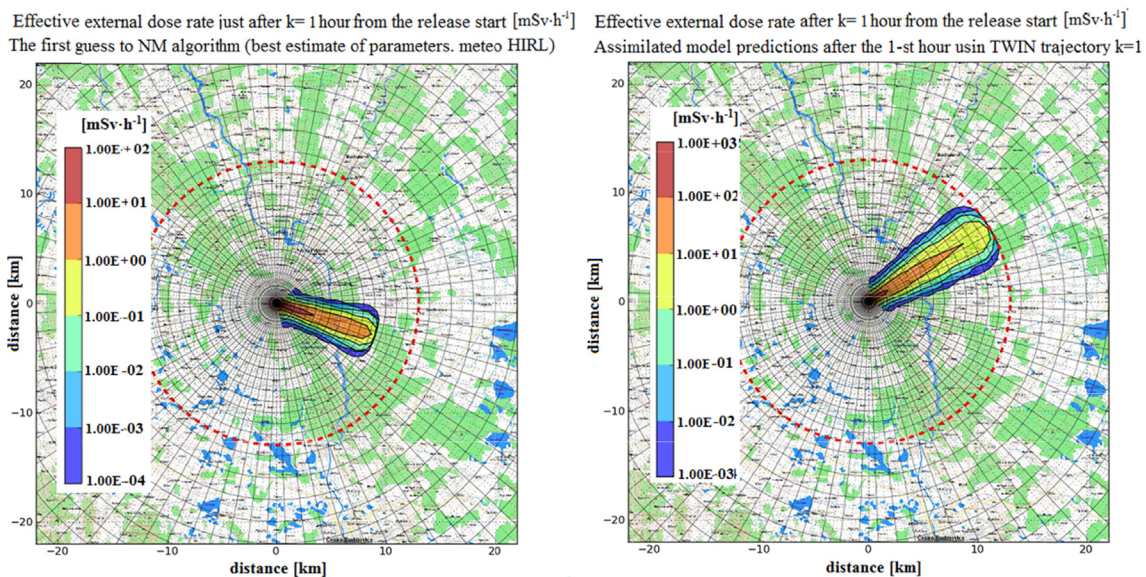


Fig. 4. Assimilation in the first hour: Left: The first guess of NM algorithm in the first hour \equiv best estimate $c_q = 1.00$, fixed $u_{10}(k=1) = u_{10}^{best} = u_{10}^{lower}$; Right: Assimilated trajectory just after 1 h: convergence reached after 124 iterations: $p = 124$, $c_q = 7.768$ (successful source term re-estimation); $c_\phi = -47.96^\circ$; $c_{u10} = 0.999$.

assimilated, fixed part of the trajectory for the first and second hours of propagation plus the best estimate of the plume segment in the 3rd hour (constructed from the parameters $c_\phi^{best}(k=3)$, $c_{u10}^{best}(k=3)$ given by the meteorological format HIRL for the centre of the nominal plume segment for $k=3$). More details are described in Appendix A. The assimilated trace on Fig. 6, right, is very close to the TWIN surface for the third hour given by sum $D = RATE_{cloud} + RATE_{ground}$ from expressions (21) which is illustrated on previous Fig. 2, left.

These procedures of recursive tracking should continue for all successive hours until the radioactive cloud leaves the considered limit 100 km from the release point. We are using the existing EWN

around nuclear facility as mentioned above. In remote distances, the number of sensors is insufficient. For testing purposes we have extended “artificially” (and subjectively) the number of measuring positions (from original 79 to 86) and assigned their corresponding TWIN values. A proper behaviour of the NM algorithm was successfully proved in the extended time span up to 8 h from the release start. The assimilated trajectory just after 8 h comes very close to the prescribed TWIN trajectory just after 8 h (see Fig. 2, Right).

4.4.3. Sensitivity study of measurement noise

Due to few available measurement sites, the measurement

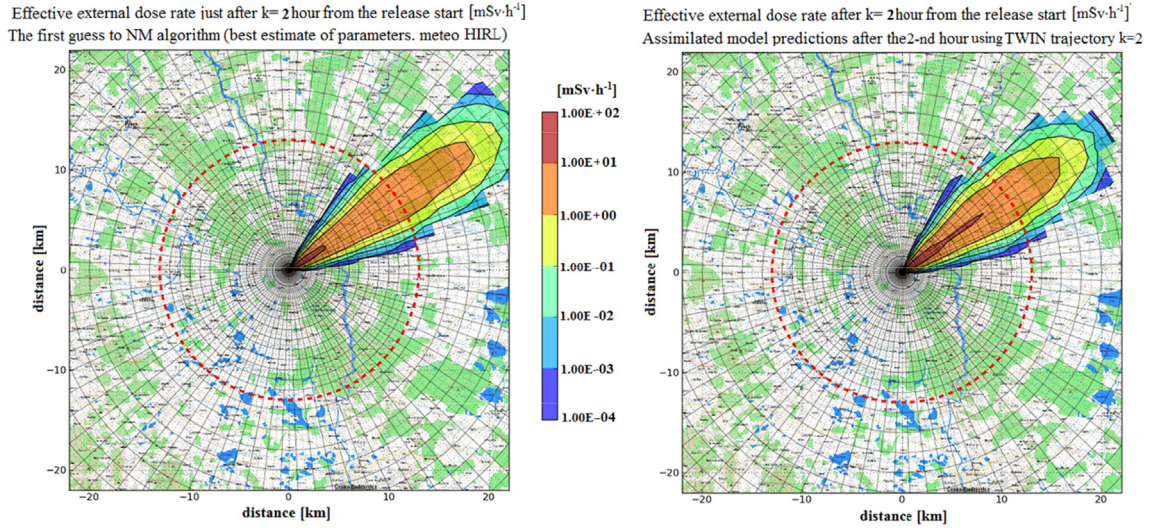


Fig. 5. Assimilation in the second hour: Left: The first guess for the 2nd hour: Trajectory of dose rate in the beginning of the minimisation procedure (1st iteration $p = 1$). Right: The convergence is reached after 95 iterations – the assimilated trajectory $\sim p = 95$, $c_q = 7.760$; $c_\varphi = -4.803^\circ$ $c_{u10} = 0.724$.

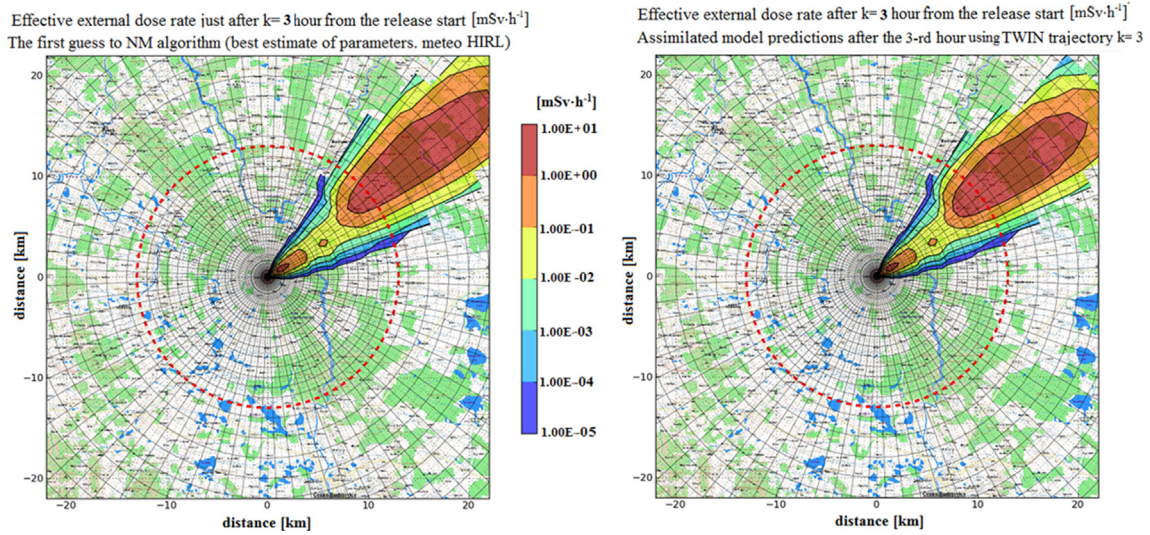


Fig. 6. Assimilation in the third hour: Left: The first guess: Trajectory of dose rate in the beginning of the minimisation procedure for $k = 3$. Right: The convergence is reached after 84 iterations – the assimilated trajectory corresponds to parameters for the third hour of the plume drifting: $c_q = 7.768$; $c_\varphi = -1.238^\circ$; $c_{u10} = 0.583$.

errors may have significant impact on the results of parameter estimation. The impact of outliers, systematic errors and stochastic uncertainties in the sensor measurements on the inverse estimation should be examined. Some assumptions on the measurement error modelling have been introduced (Abida and Bocquet, 2009; Edwards et al., 1993), more detailed observation error analysis is performed in (Edwards et al., 1993; Winiarek et al., 2011). Gaussian and non-Gaussian errors are distinguished there and a more profound analysis is provided. Common assumption is that the observation errors are not correlated and error variances are the same for the same observation type. Observation matrix C (observation error covariance matrix) can be now written as:

$$C = \sigma_{obs}^2 \cdot \begin{pmatrix} 1 & 0 & \dots & 0 \\ 0 & 1 & \dots & 0 \\ \dots & \dots & \dots & \dots \\ 0 & 0 & \dots & 1 \end{pmatrix} \quad (25)$$

We shall accept independency of the noise between measurement points r . In a particular test on correlated measurements, the identity matrix I in (25) was replaced by the actual correlation matrix for the total dependency. Expected acceleration of the minimisation NM algorithm has been achieved (the value of $P_{max}(k)$ (see (23)) was roughly about half of that valid for the case of uncorrelated measurements).

We shall perform a Monte-Carlo study of different realisation of the noise added to the simulated measurements from the TWIN experiment (Section 4.1). For each perturbed observational vector \mathbf{y}_k given (6) the optimisation (11) takes place and re-estimated parameters are produced. Specifically, the first time domain $k = 1$ is assumed (the first hour of release). We shall check the impact of the measurement noise of the dose rate on the re-estimated model parameters $q = c_q \cdot q^{best}$, $\varphi = \varphi^{best} + c_\varphi$, $u_{10} = c_{u10} \cdot u_{10}^{best}$ specified in Table 2.

In the first step the vector $\mathbf{y}_{k=1}$ (with components $y_{k=1}^r$, $r = 1, \dots, R$) of the original simulated noiseless measurements (6) of the dose rate incoming from the terrain within an hour $k = 1$ is calculated by the dispersion model. The chosen fixed TWIN values (24) are substituted into the HARP model in eq. (8). The corresponding vector of the model predictions $\tilde{\mathbf{x}}_{k=1}^{TWIN}$ in the observation space is determined using transformation (7). The noiseless measurements $\mathbf{y}_{k=1}$ are then put equal to the $\tilde{\mathbf{x}}_{k=1}^{TWIN}$. The second step follows when components of the vector $\mathbf{y}_{k=1}$ of noiseless measurements are replaced by their perturbed measurements $\hat{\mathbf{y}}_{k=1}^r$. The hat over a symbol denotes the perturbation operation.

In the absence of specific measurement campaigns, certain assumptions must be made on errors (Abida and Bocquet, 2009). We are not able to obtain a realistic measurement set which will be considered as the truth. We have tentatively introduced the test of two types of synthetic measurements: the measurement errors of the additive character and a multiplicative approach.

The **additive Gaussian type** is formed according to

$$\hat{\mathbf{y}}_{k=1}^r = \mathbf{y}_{k=1}^r + \omega^r \cdot fsig \quad (26a)$$

ω is a random number from the standard normal distribution $N(0, 1)$, factor *fsig* has a meaning of the standard deviation adjusted properly to the newly transformed normal distribution. Consequently, the loss function F from Equation (11) is rewritten as:

$$F(\hat{c}_q^p, \hat{c}_\varphi^p, \hat{c}_{u10}^p; k = 1) = \sum_{r=1}^{r=R} \left(\tilde{\mathbf{x}}_{k=1}^r(\hat{c}_q^p, \hat{c}_\varphi^p, \hat{c}_{u10}^p) - \hat{\mathbf{y}}_{k=1}^r \right)^2 \quad (26b)$$

The values $\tilde{\mathbf{x}}_{k=1}^r(\hat{c}_q^p, \hat{c}_\varphi^p, \hat{c}_{u10}^p)$ for $r = 1, \dots, R$ are components of the perturbed vector of the dose rate model predictions transformed by Equation (7) into the observation space. Subsequent searching for the minimum of the scalar function F from (26b) starts from the initial best estimate $c_q^{best}(k = 1)$, $c_\varphi^{best}(k = 1)$, $c_{u10}^{best}(k = 1)$ with the aim to re-estimate this parameter (see Appendix A). The minimisation algorithm using the loss function (26b) searches inversely the new set of perturbed parameters $\hat{c}_q^p, \hat{c}_\varphi^p, \hat{c}_{u10}^p$. The successive considerations will be focused on estimating the source release rate q modelled by $q = c_q \cdot q^{best}$ (see Table 2). Noiseless TWIN measurements are represented by the values $\tilde{\mathbf{x}}_{k=1}^{TWIN}$. The perturbed values $\hat{\mathbf{x}}_{k=1}^{TWIN}$ are labelled by hats over the symbols and result from minimisation (26b) as a function of the perturbed dose rate measurements $\hat{\mathbf{y}}_{k=1}^r$ given by (26a).

The **multiplicative error type** is formed as an alternative choice to the additive option. Multiplicative lognormal prior option is introduced for the inversion tests when the error standard deviations are fractional with respect to those of the measurements. Concurrently, we now simply assume that the dose rate measurement errors follow a lognormal law. An observation $\hat{\mathbf{y}}_{k=1}^r$ is generated from the basic noiseless data $\mathbf{y}_{k=1}^r$ multiplicatively perturbed by lognormal law:

$$\frac{\hat{\mathbf{y}}_{k=1}^r}{\mathbf{y}_{k=1}^r} = \omega_r; \omega_r \in \text{lognormal}, 3.0 - \sigma \text{ truncated} \quad (27a)$$

In this case, the cost function should be rewritten as:

$$F(\hat{c}_q^p, \hat{c}_\varphi^p, \hat{c}_{u10}^p; k = 1) = \sum_{r=1}^{r=R} \left(\ln(\tilde{\mathbf{x}}_{k=1}^r(\hat{c}_q^p, \hat{c}_\varphi^p, \hat{c}_{u10}^p)) - \ln(\hat{\mathbf{y}}_{k=1}^r) \right)^2 \quad (27b)$$

Following Section 4.4.3, the real vector $\mathbf{y}_{k=1}$ of noiseless measurements is replaced by that of the perturbed measurements $\hat{\mathbf{y}}_{k=1}$. The minimisation algorithm using loss function (27b) searches inversely for a new set of perturbed parameters $\hat{c}_q^p, \hat{c}_\varphi^p, \hat{c}_{u10}^p$. Convergence is reached after P_{max} iterations – see (23).

Both additive and multiplicative alternative priors have rather methodical purpose to demonstrate the computational feasibility and robustness. Any recommendation related to the error type option is not offered here.

4.4.4. Simulation experiment with noisy measurements

The measurement net consists of $R = 84$ sensors located on the terrain around the source of a potential radioactivity release (Fig. 3). It means that 84 independent values of the perturbation factor ω_r according to (26a resp. 27a) are generated at each sensor position and the simulation is started. The procedure is repeated 1196 times, always for a new set of perturbed measurements. The radiological consequences are estimated and processed statistically. The results are demonstrated in the form of histograms representing absolute frequencies of observations occurring in certain ranges of values. From measurement noise $\hat{\mathbf{y}}_{k=1}^r$, we have extracted information enabling us to infer on statistical properties of the random parameters represented by $\hat{c}_q^p, \hat{c}_\varphi^p, \hat{c}_{u10}^p$. The values are elementarily assumed to be the same for all nuclides *nuc* in the initial radioactivity emission (see notice in Table 2).

The efficiency of the data assimilation system is tested via statistical indicators, which introduce performance measures for comparison of the model predictions and observations. Several statistical performance measures can be used in order to compare the reference (true) plume with the reconstructed (assimilated) plume. The set of values \hat{c}_q^{itest} (*itest* = 1, ..., 1196) provides various measures of conformance. We shall mention the statistics RMSE and factor of two FAC2 and factor of five FAC5. The root mean square error (RMSE) indicator compares the source term reference with the estimated source at some time domain k :

$$RMSE = \sqrt{\frac{1}{R} \sum_{r=1}^R \left(\tilde{\mathbf{x}}_{k=1}^r(\hat{c}_q^p, \hat{c}_\varphi^p, \hat{c}_{u10}^p) - \hat{\mathbf{y}}_{k=1}^r \right)^2} \quad (28)$$

The dimensionless factors of two FAC2 resp. five FAC5 reflect the fraction r/R of data where r at a given time t satisfies:

$$0.5 \leq \frac{\tilde{\mathbf{x}}_{k=1}^r(\hat{c}_q^p, \hat{c}_\varphi^p, \hat{c}_{u10}^p)}{\hat{\mathbf{y}}_{k=1}^r} \leq 2.0 \quad \text{resp.} \quad 0.2 \leq \frac{\tilde{\mathbf{x}}_{k=1}^r(\hat{c}_q^p, \hat{c}_\varphi^p, \hat{c}_{u10}^p)}{\hat{\mathbf{y}}_{k=1}^r} \leq 5.0 \quad (29)$$

FAC n are the most robust measures, because they are not overly influenced by high and low outliers. The index $p = P_{max}$ is substituted into (28) and (29).

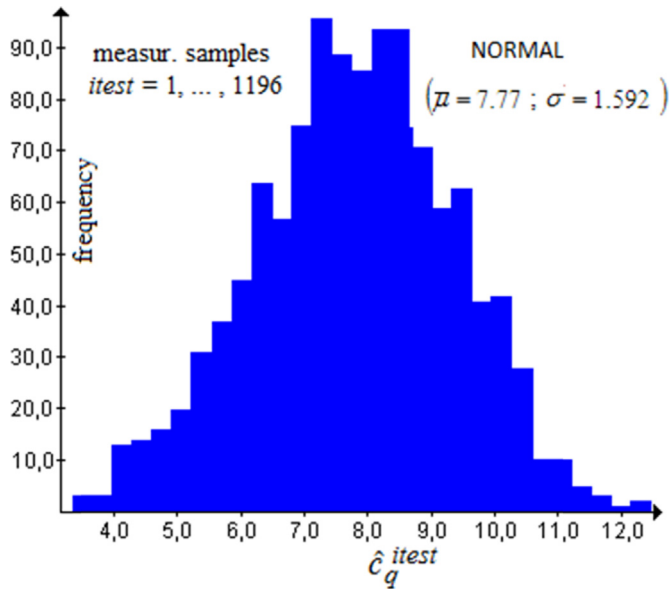


Fig. 7. Histogram for absolute frequencies of occurrence of random values \hat{c}_q^{itest} extracted from the measurement noise (Gaussian additive, CASE 1). The value 7.77 represents the noiseless chosen TWIN value $c_q^{TWIN} = 7.77$ from (24) (reference fixed value – see Section 4.4.1).

As noted above, the noise of measurements having additive or

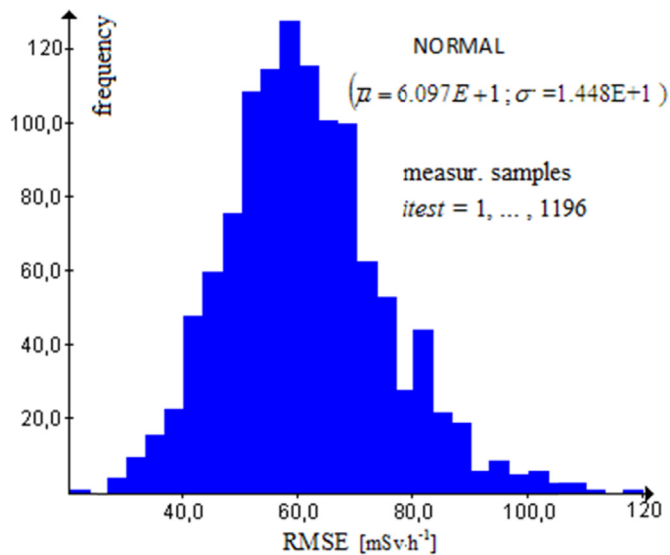


Fig. 8. Distribution of RMSE for time domain $k = 1$: Absolute frequencies of occurrence of RMSE (Gaussian additive measurement noise, CASE 1).

Table 4
Some statistical indicators for CASE 1 and CASE 2.

	CASE 1				CASE 2			
	\bar{x} (Sample mean)	σ - Sample stand. dev.	LOW conf. interval	HIGH conf. interval	\bar{x} (Sample mean)	σ - Sample stand. dev.	LOW conf. interval	HIG conf. interval
c_q	7.77E+00	1.59E+00	7.68E+00	7.86E+00	7.92E+00	1.50E+00	7.83E+00	8.01E+00
RMSE	6.10E+01	1.45E+01	6.01E+01	6.11E+01	6.38E+01	8.36E+00	6.33E+01	6.39E+01
FA2	3.21E-01	1.11E-01	3.15E-01	3.27E-01	1.07E-01	6.64E-02	1.03E-01	1.11E-01
FA5	4.92E-01	1.06E-01	4.86E-01	4.98E-01	1.61E-01	6.41E-02	1.57E-01	1.65E-01

alternatively multiplicative character has been examined. Some results follow.

4.4.4.1. Additive Gaussian type of the measurements noise. We shall distinguish between two cases of noise generation in the sensor positions:

CASE 1 Only those positions that have originally positive “artificial” noiseless measurements $\hat{x}_{k=1}^{TWIN} > 0$ are assumed. If $\hat{y}_{k=1}^r \leq 0$ is generated from (26a), then zero is substituted.

CASE 2 All sensor positions ($R = 84$ in total) are assumed regardless of their initial $\hat{x}_{k=1}^{TWIN}$ values. The noise is superimposed according to (26a) and zero is substituted here if $\hat{y}_{k=1}^r \leq 0$. This case is rather speculative and somehow simulates (in the authors’ opinion) “overall noise background”. Rather than practical results, it brings additional evidence to the computational robustness and stability.

Some results of numerical experiments on the source term reconstruction for CASE 1 just after the first hour of release propagation (time domain $k = 1$) are shown by the histogram in Fig. 7. Distribution of the sample RMSE for the first hour of release $k = 1$ is given by the histogram in Fig. 8.

Identical analysis was performed for the CASE 2. Some selected statistical indicators are summarised in Table 4 including interval estimation of the indicators (95% confidence intervals are presented – it says that interval <LOW; HIG> covers the unknown population mean value with probability 0.95).

4.4.4.2. Multiplicative type of measurement noise. In the absence of specific expert analysis of the measurement errors, an examination of alternative prior statistics on the measurements noise can bring useful information and additional verification of the algorithm. The Gaussian additive assumption is stated in the beginning of this Section. Alternatively, we have tested the lognormal prior option (27a) when the minimisation algorithm using loss function (27b) inversely searches for a new set of perturbed parameters $\hat{c}_q^p, \hat{c}_\phi^p, \hat{c}_{u10}^p$. The ratio ω from (27a) has a lognormal distribution $\omega \sim \exp(N(0, \sigma^2))$ shown in Fig. 9 (median = 1.0, $3 \cdot 0\text{-}\sigma$ truncated, the standard deviation is constructed from the given absolute quantiles Q (prob = 0.05) = 0.5; Q (prob = 0.95) = 2.0).

Some graphical results of the numerical experiments are given in Figs. 10 and 11. Interval estimates of the indicators are given in Table 5 where the 95% confidence intervals are presented. The interval <LOW; HIG> covers the unknown population mean value with probability 0.95.

5. Conclusions

A sequential minimisation scheme for recursive parameter estimation is presented here as an inverse modelling technique applied to a hypothetical accidental release of radioactivity into the atmosphere. The simulations carried out for an elementary release

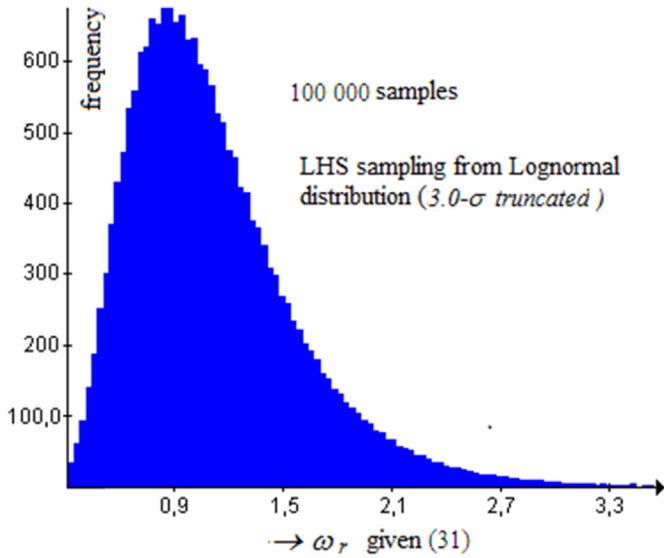


Fig. 9. Histogram for absolute frequencies of occurrence of random value ω_r driven by (27a) sampled from lognormal distribution (3.0- σ truncated).

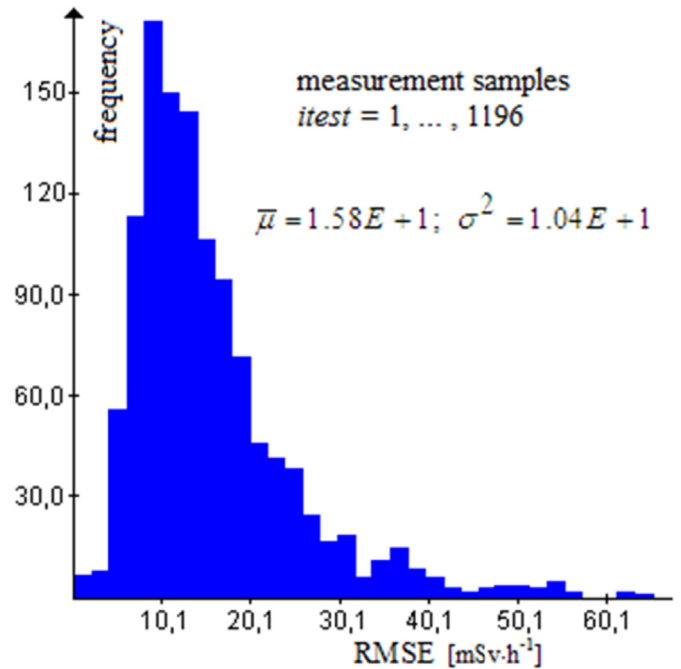


Fig. 11. Distribution of RMSE for time domain $k = 1$ (absolute frequencies of occurrence of RMSE), lognormal multiplicative perturbations of measurements given by (27a).

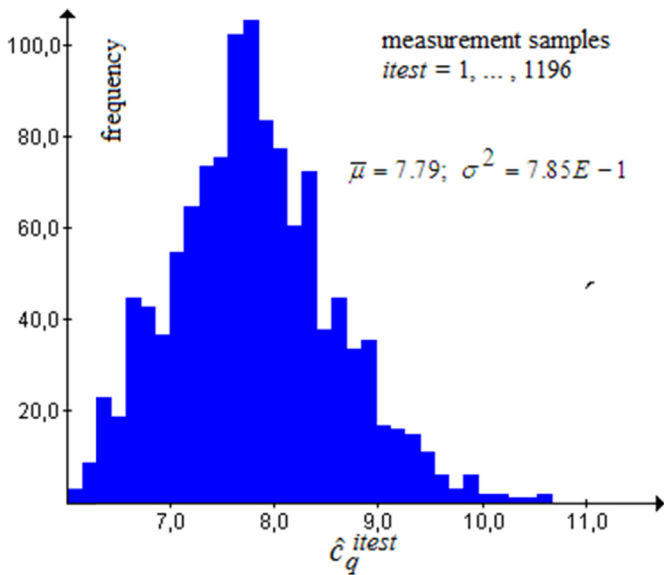


Fig. 10. Histogram for absolute frequencies of occurrence of random values \hat{c}_q^{itest} (resulted assimilation values (23)) extracted inversely from the measurement noise (lognormal multiplicative perturbations of measurements driven by (27a)). The value 7.77 represents the noiseless chosen TWIN value given by (24).

proved to be a tool useful for the improvement of the important model parameters resulting in the source strength re-estimation and recursive tracking of the radioactive plume progression. It can sufficiently contribute to the fast real-time approximation of the most impacted areas. Recursive extraction of information from the measurements allows stepwise estimation of the release dynamics. Influence of noisy measurements on the parameter estimation is examined in Sections 4.4.3 and 4.4.4. Surprising positive findings have been revealed in the optimisation using noisy measurements where the source term re-estimation is carried out simultaneously with the other wind parameters. It consists of the potential additional correction of the angular shift of the assimilated trajectory $\hat{x}_{k=1}^r(\hat{c}_q^{pmax}, \hat{c}_\phi^{pmax}, \hat{c}_{u10}^{pmax})$ from (26b) or (27b) emerging from a particular set of the measurement noise (a possibly asymmetrical random shift $c_\phi^{pmax} \rightarrow \hat{c}_\phi^{pmax}$).

Our innovative contribution includes the capability of the fast model parameter estimation for the cases of complicated multi-segment and multi-nuclide hypothetical release scenarios which can now be managed in the real-time mode. The original results lie in introducing an effective algorithm for the fast estimation of the cloudshine doses/dose rates from radioactive cloud both in its approaching and crossing phases over the sensors (Pecha and Pechova, 2014). This technique enables well-timed detection of

Table 5
95% confidence intervals for some statistical indicators – multiplicative measurement noise (27a, 27b).

	\bar{x} (Sample mean)	σ - Sample stand. dev.	LOW conf. interval	HIGH conf. interval
c_q	7.790E+00	7.849E-01	7.746E+00	7.835E+00
RMSE	1.585E+01	1.003E+01	1.528E+01	1.589E+01
FA2	2.069E-01	1.577E-02	2.060E-01	2.078E-01
FA5	2.378E-01	4.126E-03	2.376E-01	2.381E-01

the approaching radioactive plume from larger distances. Important utilisation of minimisation techniques can be found in the phase of initiation of operation of the authentic assimilation methods. Heavy computational cost of the advanced statistical techniques is caused by both enormous repetitive calling of the dispersion model and difficult setting of the proper initial approximation of the sophisticated algorithms. The improved dispersion model SGPM can provide both calculation acceleration and also delivery of a suitable guess of the intelligent initial conditions. The presented algorithm can be considered as a proper tool for verification of observability of monitoring networks.

The numerical experiment has been proven to have good computational feasibility. The minimisation procedure is fast and a real-time assimilation is fairly realisable. For multi-segment and multi-nuclide release the task is somewhat complicated but the new algorithm proposed in Section 4.3 is fully universal and practicable. The minimisation procedure BCPOL from Visual FORTRAN IMSL library proved fast convergence even for low prescribed relative error. An examination of the outlying situations has only been touched upon within the measurement noise analysis provided in Sections 4.4.3 and 4.4.4.

The presented method is based on some speculative assumptions. Sufficient temporal and spatial coverage with measuring devices is inevitable. Finer time segmentation of the release dynamics and simultaneous reduction of the recursion time step interval from one hour to 1/2 h is now being taken into consideration. An implementation of the regularisation technique for specifying constraints on the flexibility of a model can be beneficial by reducing uncertainty in the estimated parameter values (Tikhonov's regularisation: Kathirgamanathan, 2004; Winiarek et al., 2011). An unresolved problem still remains in determination of the isotopic composition of the release. The proportional representation of the particular radionuclides in the mixture could be roughly estimated from the anticipated leaking fractions of radionuclides from the core inventory. The discrimination according to a given (pre-estimated) guess can represent an alternative to the rough ad hoc choice from Scheme (22). Some partial approach for reconstruction of the isotopic composition has already been published (e.g., Saunier et al., 2013) based on analysis of the slope in the dose rate signals and peaks. However, isotopic ratios cannot be treated reasonably without spectral sensors.

Acknowledgements

The research leading to these results has received funding from the Norwegian Financial Mechanism 2009–2014 under Project Contract no. MSMT-28477/2014. Heavy computational workload was managed using simulation tool (ASIM, 2012) developed within Grant No. VG20102013018 supported by the Ministry of the Interior of the Czech Republic.

Appendix A. Stepwise recursive sequential assimilation scheme

(simplified one release segment with duration 1 h, stepwise recursion up to 8 h forward).

Initialisation phase

- Simulation of artificial “measurements” based on TWIN model using scheme (11). The TWIN data for each time step k is prepared in advance for all intended recursive time steps $k = JTWIN, JTWIN + 1, \dots, MAXTW$.

- Setup of the best estimate values of dispersion model parameters
- Selection of the most important model parameter subset to be optimised (Table 2):
 - q release source strength (Bq/h)
 - φ wind direction (deg) – angle between North and wind direction (wherefrom blows, clockwise)
 - u_{10} wind velocity (at 10 m height) (m/s)

Parameterisation of the optimisation task

Choice of vector θ from the model parameters $[c_q, c_\varphi, c_{u10}]^T$ defined as follows (Table 2):

- c_q is an unknown multiplicative factor affecting the initial best estimate source strength value q^{best} :

$$Q1 = Q1^{best} \times c_q.$$

- c_φ is an unknown additive factor affecting the nominal (forecasted) wind direction value:

$$\varphi = \varphi^{best} + c_\varphi$$

- c_{u10} is a multiplicative unknown factor affecting the nominal (forecasted) wind speed value at 10 m:

$$u_{10} = u_{10}^{best} \times c_{u10}$$

Notation

- $\{\mathbf{x}_k\}_{k=1, \dots, K}$ time evolution of the system state in discrete time domains k ; outputs from the previous step $k-1$ are predicted forward using expressions (9) and NM (Nelder-Mead) simplex method minimising (11) to the next k , taking into account the incoming observations (6).
- $JTWIN$: number of the current recursive time step being processed (the previous k time steps, $k = 1, \dots, JTWIN-1$, are assumed to be assimilated); new $JTWIN$ -th set of measurements $\mathbf{y}_{k=JTWIN}$ just arrived.
- $c_q^{asim}(k), c_\varphi^{asim}(k), c_{u10}^{asim}(k)$ are already assimilated values of the parameters in each previous recursive time steps $k, k = 1, \dots, JTWIN-1$
- $\mathbf{x}_{JTWIN-1}^{asim} \{ [c_q^{asim}(k), c_\varphi^{asim}(k), c_{u10}^{asim}(k)]_{k=1, \dots, k=JTWIN-1} \}$: assimilated 2-D plume trajectory from the same release beginning up to the $JTWIN-1$ hour. The trajectories $\mathbf{x}_{JTWIN-1}^{asim}$ are interpreted as 42×80 matrix in the computational polar nodes (42 radial distances up to 100 km from the source of pollution, 80 angular sectors).
- $\mathbf{x}_{JTWIN}^{guess} \{ [c_q^{guess}(JTWIN), c_\varphi^{guess}(JTWIN), c_{u10}^{guess}(JTWIN)] \}$: the first guess trajectory in the next $JTWIN$ -th step, which is originated during propagation of $\mathbf{x}_{JTWIN-1}^{asim}$ forward into the $JTWIN$ -th step with the initial guess $c_q^{guess}(JTWIN), c_\varphi^{guess}(JTWIN), c_{u10}^{guess}(JTWIN)$ (the guess is usually chosen as the best estimate of the parameters at the new time domain $k = JTWIN$).

Assimilation phase

- JTWIN=0
LAB: JTWIN=JTWIN+1
Action: Preparation for running model for successive hour JTWIN, read “simulated measurements” TWIN for the hour JTWIN from the external file prepared in advance
- IF (JTWIN>1) THEN
Setup initial guess trajectory $\mathbf{x}_{JTWIN}^{guess}$ for starting the assimilation process in the next JTWIN
ELSE
Guess for the first time domain TWIN=1 from:
$$\text{HARP}^{\text{SGPM}}(\theta_1^{best}, \dots, \theta_m^{best}, \dots, \theta_M^{best}; k=1) \Rightarrow \mathbf{x}_{k=1}^{best}$$
$$\mathbf{x}_{JTWIN=1}^{guess} = \mathbf{x}_{k=1}^{best}$$
ENDIF
- IF (JTWIN=1) THEN
Action: Setup CONSTRAINTS for minimisation for the first time domain JTWIN=1:
 $c_q \in \langle 0.1, 10 \rangle, c_\varphi \in \langle -90^\circ, +90^\circ \rangle, c_{u10} \in \langle 0.99, 1.01 \rangle$
where $u_{10}^{best} = u_{10}^{tow}, u_{10}^{tow}$ is onsite meteorological tower measurement of the wind speed at the time of release
ELSE
Action: Setup CONSTRAINTS for minimisation hours > 1:
 $c_q \in \langle 0.999, 1.001 \rangle, c_\varphi \in \langle -90^\circ, +90^\circ \rangle, c_{u10} \in \langle 0.5, 2.5 \rangle$
note: c_q assumed already assimilated in the first step JTWIN=1
ENDIF
- *Action: RUN optimization routine BCPOL with the evaluation function F from expression (11):*
The function $F(\theta_1, \theta_2, \dots, \theta_S)$ from (11) has now a specific form $F(c_q, c_\varphi, c_{u10})$ and minimisation algorithm handles with 3-dimensional simplex. The initial simplex for $p=1$ is assembled using the best estimate values of the vector $[c_q, c_\varphi, c_{u10}]_{best}^T \equiv [1.0, 0.0, 1.0]^T$.
 - BCPOL initialisation, $p=1$: the first iteration p of the NM minimization algorithm \equiv best estimate $[c_q, c_\varphi, c_{u10}]_{best}^T$.
L1:
 - $p=p+1$
 - NM algorithm generates the new values $(c_q^p, c_\varphi^p, c_{u10}^p)$ in the simplex vertices using JTWIN measurement set for the JTWIN-th hour
 - Generation of transient trajectory $\mathbf{x}_{JTWIN}^p(c_q^p, c_\varphi^p, c_{u10}^p)$ for p -th iteration inside the JTWIN-th time domain
 - Transformation of the $\mathbf{x}_{JTWIN}^p(c_q^p, c_\varphi^p, c_{u10}^p)$ trajectory to the observation space using observation operator - similarly to eq. (11).
 - setting logical CONV: NM algorithm itself assesses the convergence criterion
IF (.NOT. CONV) GOTO L1
 - $P_{max}(JTWIN) = p$
- *Assimilated parameters successfully found after the $P_{max}(JTWIN)$ -th iteration:*
$$\left\langle c_q^{asim}(k), c_\varphi^{asim}(k), c_{u10}^{asim}(k) \right\rangle_{k=JTWIN} \approx c_q^{P_{max}(JTWIN)}, c_\varphi^{P_{max}(JTWIN)}, c_{u10}^{P_{max}(JTWIN)}$$
- *Setup for the next recursion time step JTWIN+1 :*
IF (JTWIN ≤ MAXTW) GOTO LAB
RETURN

Appendix B. Visualisation of the Nelder-Mead (NM) algorithm – assimilation in the 3rd hour

Heuristic direct search Nelder-Mead algorithm of nonlinear optimisation technique represents a robust method for obtaining good results in many cases where a highly accurate solution is not necessary. It was shown (namely for higher number of parameters

– see Section 4.2) that significant improvement is achieved in the first few iterations. On the other side only negligible convergence or even oscillation can occur when prescribed convergence criterion is very tight and number of parameters being optimised is high. The algorithm always follows blindly the criterion of prescribed fixed lower and upper bounds on parameters. Some more sophisticated minimisation algorithm should bring benefit.

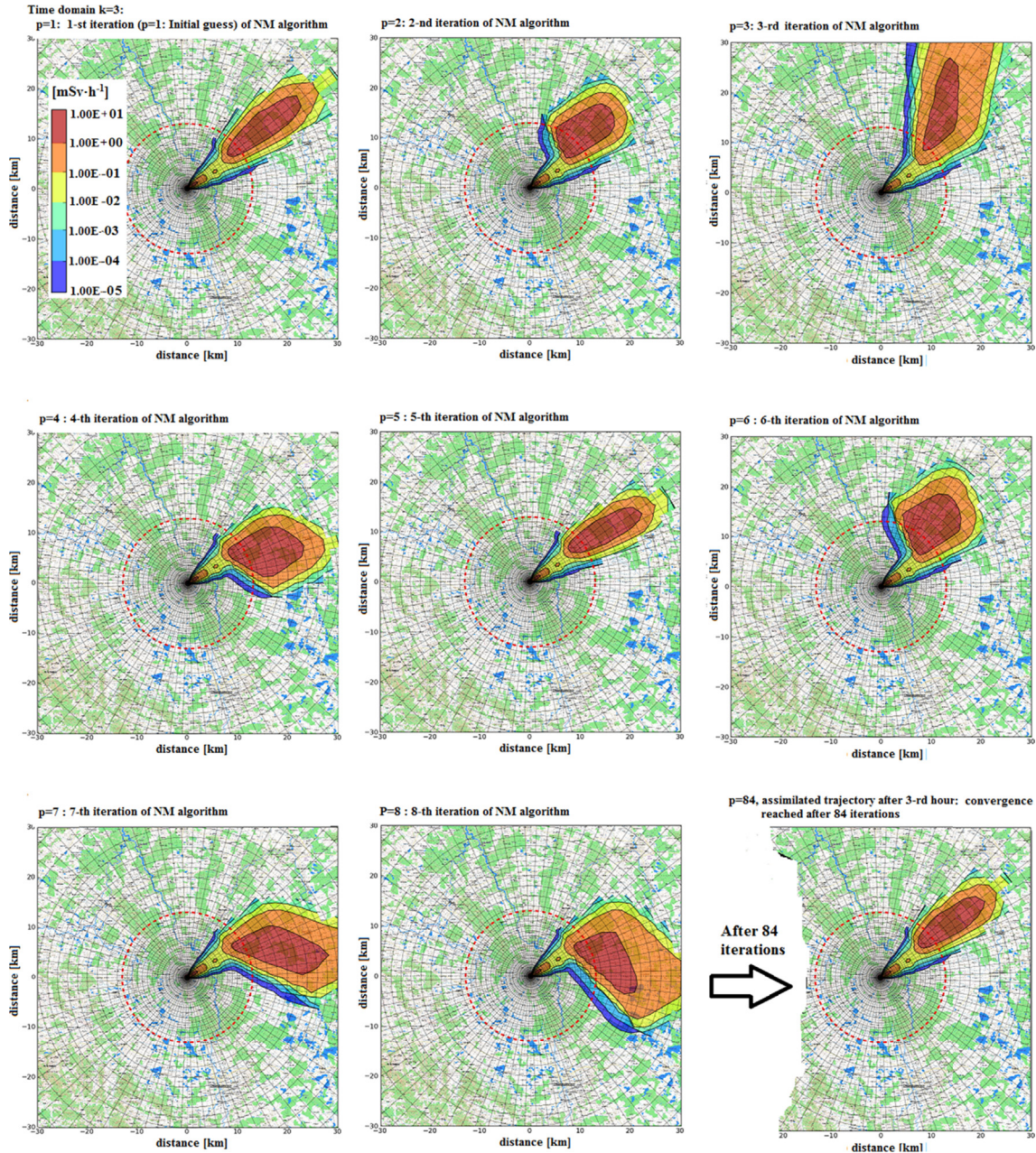


Fig. 12. Effective external dose rate [mSv h^{-1}]; Several first iterations p for assimilation in the 3rd hour. Upper left is the first guess (identical with Fig. 6, left), lower right is the assimilated trajectory after $p = 84$ iterations (identical with Fig. 6, right).

References

- Abida, R., Bocquet, M., 2009. Targeting of observations for accidental atmospheric release monitoring. *Atmos. Environ.* 43 (2009), 6312–6327.
- Andrieu, Ch., Doucet, A., Holstein, R., 2010. Particle Markov chain Monte Carlo methods. *J. R. Stat. Soc. Ser. B* (2010) 72 (Part 3), 269–342.
- ASIM, 2012. ASIM - a Software Tool for Assimilation of Model Predictions with Observations from Terrain. <http://asim.utia.cas.cz/>.
- Doucet, A., De Freitas, N., Gordon, N., 2001. *Sequential Monte Carlo Methods in Practice*. Springer Verlag.
- Edwards, L.L., Freis, R.P., Peters, L.G., Gudiksen, P.H., Pitovranov, S.E., 1993. The use of nonlinear regression analysis for integrating pollutant concentration measurements with atmospheric dispersion modeling for source term estimation. *Nucl. Tech.* 101 (No. 2), 168–180.
- HARP, 2013. HARP - Hazardous Radioactivity Propagation: a Software Tool for Fast Assessment of Radiological Consequences of Radiation Accident. <http://havarrp.utia.cas.cz/harp/>.
- Hofman, R., Pecha, P., 2011. In: Application of Regional Environmental Code HARP in the Field of Off-site Consequence Assessment. PSA 2011-International Topical Meeting on Probabilistic Safety Assessment and Analysis American Nuclear Society. IMSL library of VS FORTRAN, Wilmington, NC, USA. http://havarrp.utia.cas.cz/harp/reporty_PDF/2011/PSA_2011.PDF.
- Hofman, R., Šmídl, V., Pecha, P., 2009. Data assimilation in early phase of radiation accident using particle filter, the Fifth WMO International Symposium on Data Assimilation. In: Kepert Jeffrey, D. (Ed.), *The 5th WMO Int. Symposium on Data Assimilation*, Melbourne, AU, 05.10.2009–09.10.2009, pp. 1–8.
- Kabanikhin, S.I., 2008. 2008. Definitions and examples of inverse and ill-posed problems. *J. inverse Ill-posed Probl.* 16, 317–358.
- Kalnay, E., 2006. *Atmospheric Modeling, Data Assimilation and Predictability*. Cambridge University Press, ISBN 0-521-79179-0.
- Kathirgamanathan, P., 2004. Source parameter estimation of atmospheric pollution from accidental gas releases. In: *Int. Conf. Environmental Modelling and Software Society iEMSS*.
- Kathirgamanathan, P., McKibbin, R., McLachlan, R.I., 2003a. Inverse modelling for identifying the origin and release rate of atmospheric pollution-an optimisation approach. In: *Proceeding of. MODSIM*, 2003.
- Kathirgamanathan, P., McKibbin, R., McLachlan, R.I., 2003b. Source term estimation of pollution from an instantaneous point source. *Res. Lett. Inf. Math. Sci.* 3, 59–67.
- Krysta, M., Bocquet, M., 2007. Source reconstruction of an accidental radionuclide release at European scale. *Q. J. R. Meteorol. Soc.* 133, 529–544.
- Lee, Gab-Bock, Sohn, Wook, Yang, Zang-Hee, Park, Won-Jong, 2013. Estimation of source term by inverse model in emergency with environmental monitoring and atmospheric dispersion in Korea nuclear power plant. In: *Proceedings of the 15th Conference on Harmonisation within Atmospheric Dispersion Modelling for Regulatory Purposes*, Madrid, Spain, May 6–9, 2013.
- Pecha, P., Hofman, R., 2008. Fitting of segmented Gaussian plume model predictions on measured data. In: *Proc. of the 22th European Simulation and Modelling Conference ESM'2008*, LeHavre, FR, Oct 27–29, 2008. http://havarrp.utia.cas.cz/harp/reporty_PDF/LeHavre_RISK_02_hlava.pdf.
- Pecha, P., Pechova, E., 2014. An unconventional adaptation of a classical Gaussian plume dispersion scheme for the fast assessment of external irradiation from a radioactive cloud. *Atmos. Environ.* 89, 298–308. June 2014. http://havarrp.utia.cas.cz/harp/Photon_flux.PDF.
- Pecha, P., Hofman, R., Šmídl, V., 2009. Simulation of random 3-D trajectories of the toxic plume spreading over the terrain. In: Kepert, J.D. (Ed.), *5th WMO Symposium on Data Assimilation*. Melbourne, AU, 05.10.2009–09.10.2009. http://havarrp.utia.cas.cz/harp/reporty_PDF/WMODA2009_poster.pdf.
- Rao, K.S., 2007. Source estimation methods for atmospheric dispersion. *Atmos. Environ.* 41, 6964–6973.
- Ristic, B., Arulampalam, S., Gordon, N., 2004. *Beyond the Kalman Filter - Particle Filters for Tracking Applications*. 2004 DSTO, ISBN 978-1-58053-631-8.
- Saunier, O., Mathieu, A., Didier, D., Tombette, M., Quélo, D., Winiarek, V., Bocquet, M., 2013. Using gamma dose rate monitoring with inverse modelling techniques to estimate the atmospheric release of a nuclear power plant accident: application to the Fukushima case. In: *Proc. of the 15th Conference on Harmonisation within Atmospheric Dispersion Modelling for Regulatory Purposes*, Madrid, Spain, May 6–9, 2013.
- Šmídl, V., Hofman, R., 2014. Efficient sequential Monte Carlo sampling for continuous monitoring of a radiation situation. *Technometrics* 56 (4), 514–528. http://havarrp.utia.cas.cz/harp/reporty_PDF/2011/technometrics.pdf.
- Šmídl, V., Pecha, P., Hofman, R., 2009a. In: *Bayesian Tracking of the Toxic Plume Spreading in the Early Stage of Radiation accident*, ESM'2009-the 2009 European Simulation and Modelling Conference, Modelling and Simulation, pp. 381–387. Leicester, GB, 26.10.2009–29.10.2009. http://havarrp.utia.cas.cz/harp/reporty_PDF/Total_ESM2009.pdf.
- Šmídl, V., Hofman, R., Pecha, P., 2014. Evaluation of detection abilities of monitoring networks using multiple assessment criteria. *Int. J. Environ. Pollut.* 129–138. http://havarrp.utia.cas.cz/harp/reporty_PDF/2013/IJEP_2013.pdf.
- Stohl, A., Seibert, P., Wotawa, G., Arnold, D., Burkhardt, J.F., Eckhardt, S., Tapia, C., Vargas, A., Yasunari, T.J., 2012. Xenon-133 and caesium-137 releases into the atmosphere from the Fukushima Dai-ichi nuclear power plant: determination of the source term, atmospheric dispersion, and deposition. *Atmos. Chem. Phys.* 12, 2313–2343. <http://dx.doi.org/10.5194/acp-12-2313-2012>.
- Talagrand, O., 1997. Assimilation of observations, an introduction. *J. Meteorol. Soc. Jpn.* 75 (1B), 191–209.
- Winiarek, V., Vira, J., Bocquet, M., Sofiev, M., Saunier, O., 2011. Towards the operational estimation of a radiological plume using data assimilation after a radiological accidental atmospheric release. *J. Atmos. Environ. Elsevier* 45 (17), 2944–2955.
- Winiarek, V., Vira, J., Bocquet, M., Saunier, O., Mathieu, A., 2012. Estimation of errors in the inverse modeling of accidental release of atmospheric pollutant: application to the reconstruction of the cesium-137 and iodine-131 source terms from the Fukushima Daiichi power plant. *J. Geophys. Res. Atmos. Am. Geophys. Union* 117.